American Journal of Energy Research, 2025, Vol. 13, No. 2, 26-64
Available online at http://pubs.sciepub.com/ajer/13/2/1
Published by Science and Education Publishing
DOI:10.12691/ajer-13-2-1

Optimum Model of a Solar Desalination System based on Multi-effect Distillation (Solar-MED)

Behrooz Heidari Dehkordi[1], Fatemeh Saberi[2,*], Abtin Ataei[3], Hossein Salehfar[4], Farhad Abdollahzadeh Bina[5]

[1]Department of Mechanical Engineering, North Dakota State University, Fargo, ND, USA
[2]Department of Energy & Petroleum Engineering, University of North Dakota, Grand Forks, ND, USA
[3]School of Engineering, University of Dayton, Dayton, USA
[4]UND School of Electrical Engineering and Computer Science, Grand Forks, USA
[5]Department of Geology and Geological Engineering, University of North Dakota, Grand Forks, ND 58202, USA
*Corresponding author: Fatemeh.saberi@ndus.edu

Received April 28, 2025; Revised May 29, 2025; Accepted June 06, 2025

Abstract This study evaluates the performance of Multi-Effect Distillation (MED) and Multi-Stage Flash (MSF) desalination systems integrated with solar energy and conventional boilers. Simulations using numerical software modeled all systems to produce 1200 cubic meters of freshwater per day under similar conditions along the Persian Gulf coast. Results indicate that system type and energy source significantly affect costs, efficiency, and sustainability. The MED-Solar Field system emerged as an economically viable and eco-friendly option, with a production cost of \$3.22 per cubic meter in the first year and reduced emissions. The MED-Conventional Boiler system had the lowest cost (\$1.55/m³) but relied on fossil fuels. The MSF-Solar Field system, with a high cost of \$7.93/m³, was deemed unfeasible due to substantial initial investment. The MSF-Conventional Boiler system, with a cost of \$4.66/m³ and high efficiency (85%), demonstrated reasonable economic performance but posed environmental concerns. The study also analyzed the effects of environmental factors on solar system efficiency to enhance future designs. These findings offer insights for selecting optimal desalination technologies across climates, promoting renewable energy integration, cost reduction, and advancing water and energy resource management.

Keywords: *MED-Solar Field system, MED-Conventional Boiler system, MSF-Solar Field system, MSF-Conventional Boiler system, optimization, sensitivity analysis*

Cite This Article: Behrooz Heidari Dehkordi, Fatemeh Saberi, Abtin Ataei, Hossein Salehfar, and Farhad Abdollahzadeh Bina, "Optimum Model of a Solar Desalination System Based on Multi-effect Distillation (Solar-MED), Iran." *American Journal of Energy Research*, vol. 13, no. 2 (2025): 26-64. doi: 10.12691/ajer-13-2-1.

1. Introduction

The study of Solar-MED (Multi-Effect Distillation) is crucial due to the increasing global water scarcity and the need for sustainable, energy-efficient desalination solutions. As freshwater resources are limited, especially in arid regions, desalination has become a vital method for ensuring water security. However, conventional desalination processes are energy-intensive and costly. Solar-MED offers a promising alternative by utilizing solar energy, a renewable and abundant resource, to power the desalination process, significantly reducing dependence on fossil fuels and lowering operational costs [1,2,3]. The integration of solar energy into desalination systems enhances their sustainability, making Solar-MED a key solution for addressing water scarcity in regions like the Middle East and North Africa, where desalinated water provides a significant portion of potable water [7,16,21]. The development of solar desalination technologies has been the subject of extensive research over the years. One of the earliest methods explored was the solar still, which operates by utilizing the sun's heat to evaporate water, leaving the salts behind, and then condensing the vapor to produce fresh water. While single-slope solar stills were initially studied, researchers have since advanced to double-slope solar stills to increase distillation efficiency [4,5]. Further innovations include the use of wick materials to enhance evaporation rates and the application of deep machine learning algorithms to optimize solar still designs for better performance and lower costs [6-17]. Additionally, vacuum-based desalination systems have been explored to improve efficiency by utilizing waste heat from steam turbines [18]. This approach was first tested in 1991 by Low and Tay, who successfully demonstrated the feasibility of vacuum desalination using seawater [9,15,19,37]. The introduction of ejectors in desalination systems has also contributed to optimizing energy use. Ejectors are employed to maintain vacuum pressure in the system, reducing the need for high-grade energy-consuming pumps. For instance, [20] designed and tested a two-phase ejector for desalination systems, which significantly improved the vacuum performance while maintaining energy efficiency [20-29] Furthermore, researchers have developed hybrid solar cells and new materials to enhance the efficiency of photovoltaic systems that power solar desalination systems. These advancements, such as the use of perovskite-based solar cells and monocrystalline silicon solar cells, have led to improvements in solar power generation, further enhancing the performance of solar desalination systems [8,21,22,23,24]. Using renewable energy (RE) to power desalination processes is a sustainable solution to provide potable water in water-scarce regions [1]. Solar energy is the most abundant renewable energy source and is highly suitable for powering both thermal and membrane processes. Thermal processes include multi-stage flash (MSF), multi-effect distillation (MED), thermal vapor compression (TVC), and mechanical vapor compression (MVC). Several studies have highlighted the importance and suitability of solar desalination for the Middle East and North Africa (MENA) region, one of the world's most water-scarce regions [7,14,25,26,27]. The coupling of solar energy technologies, such as concentrated solar power (CSP), with thermal desalination is still in the research and development (R&D) phase, requiring extensive research in this field [28,30,32,33,34]. Numerous studies have investigated the challenges and opportunities for ensuring that solar energy-powered desalination is feasible [29-34]. Among current solar desalination technologies, solar-thermal-driven multi-effect distillation (MED) may be the most suitable for large-scale implementation owing to its superior thermodynamic and heat transfer performances compared to the MSF process and its lower levelized cost of water (LCOW) [35-39]. Building on this, it is reasonable to argue that solar-driven MED is the most suitable thermal desalination technology for large-scale seawater desalination, as also highlighted by [40]. Therefore, this article aims to introduce an innovative approach to seawater desalination by integrating multi-effect distillation (MED) and flash evaporation methods within a solar-powered cogeneration system [41,36,45,46]. The study focuses on developing an optimal model using numerical software to evaluate the system's performance and conducting a comprehensive sensitivity analysis to enhance energy efficiency and system design. By comparing the costs and efficiencies of the proposed solar-MED and flash evaporation systems with conventional desalination methods, this research seeks to demonstrate the viability and sustainability of solar-based technologies as a promising solution for freshwater production in the context of increasing global water scarcity [10,11,12,13,44].

2. Method

In this study, a comprehensive and detailed approach is applied to analyze and compare different desalination systems. For this purpose, numerical software is used as the main tool for simulation and analysis. This software is selected due to its extensive capabilities in modeling energy and thermal systems, making it ideal for performing precise analyses of various systems, particularly in desalination and assessing their performance. Initially, four distinct systems are considered, each with its specific characteristics. These systems are: the MED-Solar Field, which utilizes the MED (Multi-Effect Distillation) technology combined with a solar field for thermal energy supply; the MED-Conventional Boiler, where the same MED technology is employed, but instead of solar energy, a conventional boiler is used for thermal energy generation; the MSF-Solar Field, which is based on the MSF (Multi-Stage Flash Distillation) process, also utilizing a solar field for energy provision; and the MSF-Conventional Boiler, which is similar to the previous system but uses a conventional boiler instead of solar energy for thermal supply. To ensure an accurate comparison of the systems, four units with a capacity of 1200 m^3/day of freshwater production are used under identical environmental conditions. The environmental conditions, extracted from the Table 1 for the Persian Gulf coastline, are consistently applied to all models. These conditions include temperature, humidity, and solar radiation, which significantly affect the performance of desalination systems [17,18,38]. In this step, each of the systems is modeled within numerical software. All input parameters, such as temperature, pressure, and fluid properties, are defined. Then, the systems are simulated independently to thoroughly assess the performance of each system. After the initial modeling, to ensure the correctness of the design and the software's functionality, the system is switched to Engineering Mode. In this mode, the initial design is executed, and potential errors are identified and rectified. This step helps refine the system towards real operational conditions. After confirming the accuracy of the design and functionality of the systems, the analysis proceeds to the OFF Design mode for sensitivity analysis. In this mode, various input parameters, such as temperature, pressure, and fluid properties, are altered, and the impact of these changes on the system's output parameters (such as freshwater production) is calculated. This analysis helps assess the system's sensitivity to environmental and operational variations, providing a deeper understanding of its performance under different conditions. Subsequently, the results from the simulations for each system are collected and compared. This comparison involves evaluating freshwater production, energy consumption, operational costs, and system efficiency under varying conditions. The final results are comprehensively analyzed to select the optimal system for specific conditions [19,20,40,43]. Finally, after completing the simulations and analyzing the results, the study concludes by identifying the most efficient system for freshwater production under the given environmental conditions. This conclusion can serve as a reference for designing similar systems in other regions. This study method comprehensively covers all stages, from design to sensitivity analysis and system comparison, providing an in-depth assessment of the performance of different desalination systems [31,37,41,42].

Table 1. Environmental and Operational Parameters

Parameter	Value	Unit
Site Altitude	5	m
Ambient Temperature	35	°C
Ambient Relative Humidity	60	%
Ambient Wet Bulb Temperature	28.18	°C
Ambient Pressure	1.014	bar
Latitude	25.25N	-
Longitude	55.33E	-
Minimum Dry Bulb Temperature	9.7	°C
Maximum Dry Bulb Temperature	45.5	°C
Direct Normal Irradiance	800	W/m²
NaCl Weight Percent	4	%

3. Discussion and Results

3.1. Performance Analysis of MED and MSF Systems with Solar and Boiler Energy

In this section, four systems, including MED-Solar Field, MED-Conventional Boiler, MSF-Solar Field, and MSF-Conventional Boiler, were modeled using the numerical software. These systems were analyzed with a focus on different thermal energy sources (solar field and conventional boiler) and technologies (MED and MSF) to evaluate their performance and efficiency, with the details presented in the following sections.

3.1.1. MED Solar Field System

The MED-Solar Field system, schematically illustrated in Figure 1, employs inlet steam (13287 kW), seawater feed (10769 kW), and a pump (62 kW) as energy inputs, while condenser return (927 kW), cooling water discharge (13666 kW), desalinated water (3106 kW), blowdown (5768 kW), and heat loss (652 kW) constitute its energy outputs; these values are reported in Table 1 and reflect the overall energy balance throughout the various stages and components of the MED desalination unit, along with its operating costs. System specifications—including the number of units, number of effects, dimensions, and unit prices—are summarized in Table 2. In contrast, Table 3 presents both general and specific characteristics of the effects and the condenser employed in this project. The heat transfer fluid in the solar field is Therminol VP-1, which remains in liquid phase at all process stages; the corresponding thermal balance and solar irradiation data are provided in Table 4. Table 5 details the design parameters of the collectors, receivers, and other hardware in the solar field, indicating a 75% optical efficiency and a receiver tube with an outer diameter of 70 mm and an inner diameter of 67/64 mm, fabricated from TP321H. The solar field occupies an approximate area of 43000 m², as shown in Table 6, along with the associated operational costs. To supply electricity for the system's pumps and other components, a steam turbine—whose operational parameters are given in Table 7—receives superheated steam at 10 bar and 400°C from the solar field heat exchanger and exhausts at 2.5 bar and 300°C. To determine the water production cost, the total project expenditure was calculated using numerical software, with a summary of the costs in Table 8 and a breakdown of each component's price in Table 9. The fixed project costs amount to USD 35106927, while fixed and variable maintenance costs are USD 20/kW and USD 0.001/kW, respectively. Given a net power output of 2.458 kW and a 25-year design life, the first-year water production cost is estimated to be USD 3.22 per cubic meter.

3.1.2. MED-Conventional Boiler System

The MED-Conventional Boiler system in this project is meticulously designed to maintain all parameters of the desalination unit, including the steam turbine, MED unit, condenser, pumps, and cooling tower, in a fixed state. Instead of utilizing a solar cycle, the required steam is supplied by the boiler, as depicted in the schematic diagram shown in Figure 2. The boiler employed in this setup operates on methane fuel, and its fuel specifications are detailed in Table 10. The higher heating value of methane gas at 25°C is considered to be 50,047 kJ/kg. This boiler operates with 15% excess air and achieves an efficiency of approximately 81%. The thermal balance of the boiler is presented in Table 11, while the technical specifications and pricing information are available in Table 12. Additionally, Table 13 provides data on temperature, pressure, flow rate, and enthalpy of water/steam at various stages of the boiler. To calculate the cost of water production for this project, it is essential to determine the total cost of the design, which is performed using the numerical software. A summary of the costs is provided in Table 14, and the total cost for each component of the project in USD is available in Table 15. Based on the fixed costs outlined in the aforementioned tables, the cost per cubic meter of water is calculated as follows:

- Fixed Costs: USD 8,515,818
- Fixed Maintenance Costs: USD 20 per kW
- Variable Maintenance Costs: USD 0.01 per kW
- Fuel Cost for the First Year [https://www.naftnews.ir]: USD 0.25 per m³

The annual fuel cost is calculated using the following formula:

Annual Fuel Cost = 0.025 $/m3×0.2979 kg/s×(10.717 m3/kg) ×3600×24×365=327,565 $

Considering that the system generates 2,458 kW of electricity and has a design life of 25 years, the cost per cubic meter of produced water in the first year is determined to be USD 1.55. These calculations demonstrate that utilizing a methane-fired boiler within the MED-Conventional Boiler system enables the production of water at an optimized and cost-effective rate. All data related to the boiler's performance and associated costs are comprehensively presented in the referenced tables, facilitating a detailed analysis of the system's efficiency and economic viability.

3.1.3. MSF Solar Field System

The MSF Solar Field system is illustrated in Figure 3. In designing this system, the use of steam at higher pressure and temperature, compared to the MED system, necessitates the incorporation of two turbines: one positioned upstream and the other downstream of the MSF unit. Additionally, the condensed water in the condenser has a higher temperature than the feedwater, which requires the implementation of a heat exchanger to utilize this thermal energy effectively. Moreover, the expanded steam from the second turbine cannot be released into the atmosphere due to environmental and energetic constraints; therefore, an additional condenser and cooling tower are employed. The specifications of the MSF unit used are detailed in Table 16. Given the extensive and complex nature of the MSF unit, the thermal balance results of the examined design, considering all heat transfer sources within the unit, are provided in Table 17. The specifications of the MSF unit, including capacity, number of stages, type of stages, dimensions, costs, and other pertinent details, are presented in Table 18. The heat transfer fluid utilized in the solar field is Therminol VP-1, which remains in liquid form throughout all operational stages. The thermal balance of the solar field is shown in Table 19, along with the solar irradiance entering the collector array. The hardware specifications of the solar field are outlined in Table 20, encompassing an area exceeding 151,000 square meters and a structural weight of approximately 1,300 tons, as detailed in Table 21. To determine the cost of the produced water from this project, the total cost of the design must be calculated, which is achievable using numerical software. The summarized costs are presented in Table 22. Additionally, the software is capable of providing the total cost of each component in USD, as listed in Table 23. As indicated in the system schematic, the MSF process requires the use of additional components, including a steam turbine costing $3,000,000, a water-cooled condenser costing $757,643, and a wet cooling tower costing $739,531, resulting in an additional approximately $5.4 million for these equipments. Furthermore, due to the higher energy demand in MSF units, which is inherently greater than that of MED units in medium-sized sites, the initial investment for the Solar Field in this unit is significantly higher than that of a comparable MED unit. Considering the abovementioned costs, the price per cubic meter of produced water is calculated as follows: fixed costs amount to $81,733,940, fixed maintenance costs are $20 per kW, and variable maintenance costs are $0.01 per kW. With an electricity generation capacity of 10,240 kW and a system design life of 25 years, the cost per cubic meter of produced water in the first year is $7.93 USD/m³.

3.1.4. MSF Conventional Boiler System

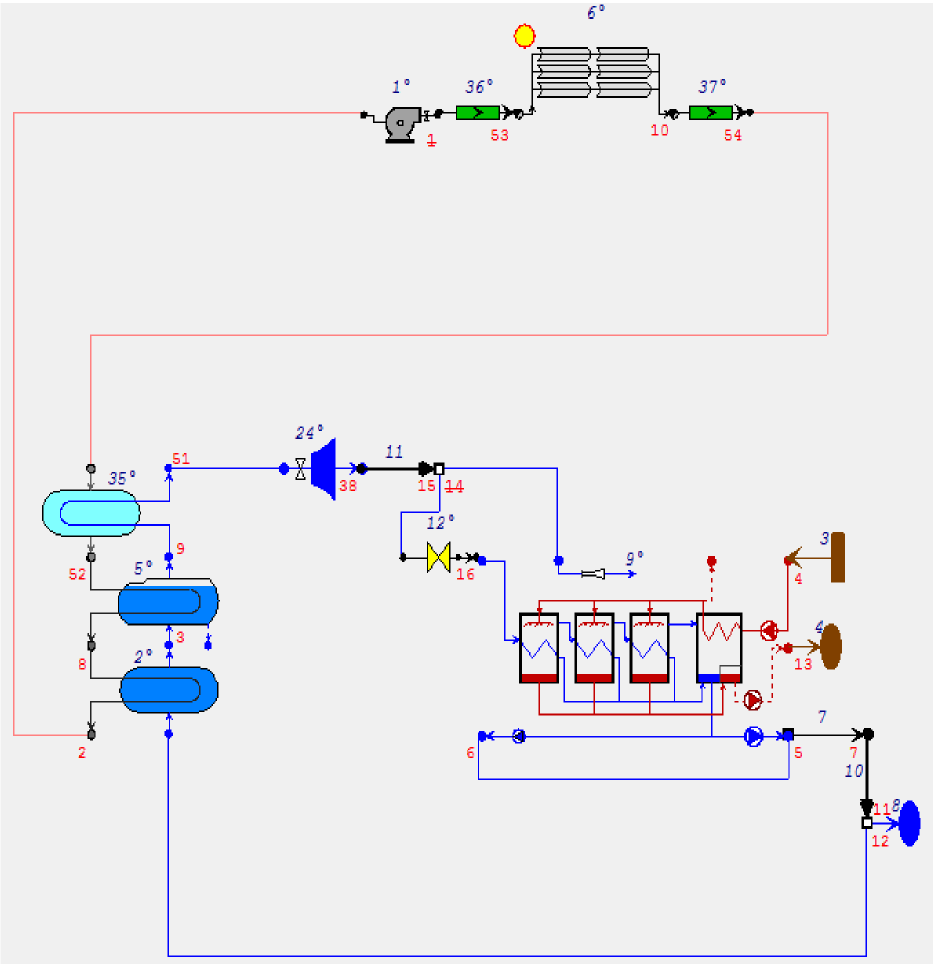

Figure 1. Schematic diagram of the MED-Solar system utilized

The MSF conventional boiler system, depicted in Figure 4, has been examined in this study. Given that all related tables and figures were reviewed in the previous section and only the boiler has been substituted for the solar field circuit, our focus is entirely on the tables and figures pertaining to the boiler. The boiler in use operates with 15% excess air and has an approximate efficiency of 85%. The thermal balance of this boiler is presented in Table 24, and its specifications, including cost, are detailed in Table 25. Additionally, Table 26 provides information on temperature, pressure, flow rate, and enthalpy of water/steam at various stages of the boiler. The thermal energy produced by the boiler as a function of temperature is clearly illustrated in the T-Q diagram shown in Figure 5. To determine the cost of water production from this project, it is necessary to calculate the total cost of the design, which can be performed using numerical software. A summary of the costs is presented in Table 27, and the software also calculates the total cost of each component in US dollars (USD), which are provided in Table 28. The fixed costs of the project are established at USD 18,457,800. Additionally, fixed maintenance costs amount to USD 20 per kW, and variable maintenance costs are USD 0.01 per kW. The fuel cost for the first year is set at USD 0.025 per cubic meter, calculated as follows:

Fuel cost for 1 year = 0.025 USD / $m^3\times$ 1.004 kg/s$\times$10.717 m^3/kg$\times$3600$\times$24$\times$365 = 1,103,979 USD

Considering that the electricity production in the system is 10,040 kW and the system's design lifespan is 25 years, the cost per cubic meter of water produced in the first year is USD 4.66.

Table 2. Energy Balance for the MED Unit

		Off-design Heat Balance Results
		MED Desalination[9]
	1	Number of units
	3.351	Gain output ratio (desalinated water / steam flow)
	2.751	Performance ratio (kg/2325.9kJ)
		Desalinated Water
bar	10.06	Pressure
C	53.38	Temperature
kJ/kg	224.2	Enthalpy
kg/s	13.85	Mass flow (per unit)
MIGD	0.264	Volume flow (MIGD per unit)
m^3/day	1200	Volume flow (m^3/day per unit)
kg/s	13.85	Mass flow (total)
MIGD	0.264	Volume flow (total, MIGD)
m^3/day	1200	Volume flow (total, m^3/day)
		Heating Steam Supply
bar	3.447	Pressure
C	293.8	Temperature
kJ/kg	3057	Enthalpy
kg/s	4.133	Mass flow (per unit)
kg/s	4.133	Mass flow (total)
		Steam Supply to Vacuum System
bar	5.2	Pressure
C	296.3	Temperature
kJ/kg	3057	Enthalpy
kg/s	0.2132	Mass flow (per unit)
kg/s	0.2132	Mass flow (total)
		Desuperheating Water (from Condensate Return Line)
kg/s	0.7154	Mass flow (per unit)
kJ/kg	224.2	Enthalpy
		Steam at First Effect Inlet
bar	0.3117	Pressure
C	75	Temperature
kJ/kg	2639.3	Enthalpy
kg/s	4.848	Mass flow (per unit)
		Condensate Return

bar	10.06	Pressure
C	53.34	Temperature
kJ/kg	224.2	Enthalpy
kg/s	4.133	Mass flow (per unit)
kg/s	4.133	Mass flow (total)
		Seawater Supply
bar	1.014	Pressure
C	25	Temperature
%	4	Salt concentration
kJ/kg	99	Enthalpy
kg/s	108.8	Mass flow (per unit)
kg/s	108.8	Mass flow (total)
		Cooling Water Discharge
bar	1.014	Pressure
C	51.23	Temperature
%	4	Salt concentration
kJ/kg	203.3	Enthalpy
kg/s	67.23	Mass flow (per unit)
kg/s	67.23	Mass flow (total)
		Brine Blowdown
bar	1.014	Pressure
C	53.96	Temperature
%	6	Salt concentration
kJ/kg	208.2	Enthalpy
kg/s	27.7	Mass flow (per unit)
kg/s	27.7	Mass flow (total)
		Main Condenser Cooling Water Inlet
bar	2.289	Pressure
C	25.04	Temperature
%	4	Salt concentration
kJ/kg	99.28	Enthalpy
kg/s	108.8	Mass flow (per unit)
		Main Condenser Cooling Water Exit
bar	2.068	Pressure
C	51.21	Temperature
kJ/kg	203.3	Enthalpy
kg/s	108.8	Mass flow(per unit)
kg/s	41.55	- Mass flow to feed evaporator (per unit)
kg/s	67.23	- Mass flow to discharge (per unit)
		Chemical Consumption (100% equivalent)
kg/hr	0.3739	Anti-scale
kg/hr	4.487	Sulfuric acid
kg/hr	0.4986	Caustic soda
kg/hr	0.1994	Chlorine
USD	39840	Total O&M cost per year
kW	89.92	Power Consumption (plant total)
kW	89.92	Power Consumption (per unit)
kW	68.8	- Pumps
kW	21.12	- Miscellaneous auxiliaries
kW	24118	Energy In (total)
kW	13287	- Steam supply

kW	10769	- Seawater supply
kW	61.92	- Pump work
kW	24118	Energy Out (total)
kW	926.7	- Condensate return
kW	13666	- Colling water discharge
kW	3106	- Desalinated water
kW	5768	- Blowdown
kW	651.7	- Heat loss
%	0	Heat Balance Error

Table 3. Specifications of the MED Unit Used

		Estimated Multi-Stage Flash (MED) Desalination System Data
		MED Desalination[9]
	Off Design	Computation mode
		1. General
	1	Number of units
	3	Number of effects per unit
	MED only	System configuration
C	70	First effect heating steam saturation temperature
C	66.16	Top brine temperature
C	55.01	Final effect temperature
kg/s	13.85	Nameplate capacity
MIGD	0.264	Nameplate capacity (MIGD)
m^3/day	1200	Nameplate capacity (m^3/day)
		2. Evaporator island (per unit, incl. main condenser)
m^2	3568	Total heat transfer area
M	19.39	Length
M	8.992	Width
M	5.095	Height
tonne	53.37	Dry weight
tonne	74.64	Operating weight
		3. Evaporators (per unit)
m^2	2988.4	Total heat transfer area
	3	Number of effects
m^2	996.1	Heat transfer area per effect
	6293	Number of tubes per effect
mm	15.88	Tube outside diameter
mm	0.508	Tube wall thickness
M	3.174	Tube length
	Titanium	Tube material
tonne	2.304	Tube dry weight per effect
M	15.23	Total shell length of all effects
M	2.997	Shell outside diameter
mm	9.525	Shell wall thickness
tonne	6.913	Total tube dry weight
tonne	31.98	Total dry weight
tonne	53.35	Total operating weight
tonne	137.8	Total flooding weight
		4. Main condenser (per unit)
M	7.097	Overall length
M	1.11	Overall width

M	1.858	Overall height
m^2	579.9	Heat transfer area
	2208	Number of tubes
	2	Number of passes
mm	12.7	Tube outside diameter
mm	0.5588	Tube wall thickness
M	6.582	Tube length
	Titanium	Tube material
tonne	1.457	Tube dry weight
tonne	5.882	Total dry weight
tonne	8.857	Total operating weight
		5. Cost Summary
USD	2,684,503	Total reference installed cost
	1	Total installed cost adjustment factor
USD	2,727,456	Total estimated installed cost

Table 4. Specifications of the Condenser and Effects in the MED System

					MED Effects/Condenser Data
					MED Desalination[9]
			Design	Off	Computation mode
Condenser	Effect 3	Effect 2	Effect 1		
					General
0.144	0.144	0.190	0.246	Bar	Pressure
53.2	55.0	60.7	66.2	C	Temperature
	0.72	0.75	0.78	C	Boiling point elevation
	1.06	0.95	0.74	C	Non-equilibrium
1974.2	2642.3	2795.4	2975.6	W/m^2-C	Overall heat transfer coefficient
11312.0	10601.0	10887.0	11375.0	kW	Heat transfer in evaporator
	0.0	652.8	0.0	kW	Heat transfer in preheater
					Steam In
0.144	0.190	0.246	0.312	Bar	Pressure
55.0	60.7	66.2	75.0	C	Temperature
53.2	59.0	64.6	70.0	C	Saturation temperature
4.56	4.48	4.63	4.85	kg/s	Mass flow
2604.2	2613.6	2622.5	2639.3	kJ/kg	Enthalpy
					Brine In
0.144	0.190	0.246		Bar	Pressure
55.0	60.7	66.2		C	Temperature
5.99	5.96	5.93		%	Salt concentration
27.8	18.9	9.6		kg/s	Mass flow
212.30	234.80	256.10		kJ/kg	Enthalpy
					Condensate In
0.190	0.190	0.312		Bar	Pressure
59.0	59.0	70.0		C	Temperature
14.1	9.6	4.8		kg/s	Mass flow
246.90	246.80	293.00		kJ/kg	Enthalpy
					Feedwater In
	2.1	2.1	2.1	Bar	Pressure
	51.2	51.2	57.0	C	Temperature
	4.00	4.00	4.00	%	Salt concentration
	41.6	28.1	14.2	kg/s	Mass flow
	203.30	203.30	226.50	kJ/kg	Enthalpy
					Feedwater to Evaporator
	2.1	2.1	2.1	Bar	Pressure

	51.2	57.0	57.0	C	Temperature
	4.00	4.00	4.00	%	Salt concentration
	13.4	13.9	14.2	kg/s	Mass flow
	203.30	226.50	226.50	kJ/kg	Enthalpy
					Feedwater Exit
	2.1	2.1		Bar	Pressure
	51.2	57.0		C	Temperature
	4.00	4.00		%	Salt concentration
	28.1	14.2		kg/s	Mass flow
	203.30	226.50		kJ/kg	Enthalpy
					Flash from Feed
	4.38	4.53	4.63	kg/s	Mass flow
	2604.2	2613.7	2622.5	kJ/kg	Enthalpy
					Flash from Brine
0.05	0.18	0.09		kg/s	Mass flow
2600.4	2604.3	2613.8		kJ/kg	Enthalpy
					Flash from Condensate
0.14	0.00	0.14		kg/s	Mass flow
2597.7	0.0	2607.8		kJ/kg	Enthalpy
					Steam to Preheater
	0.144	0.190		Bar	Pressure
	0.00	0.27		kg/s	Mass flow
	2604.2	2613.6		kJ/kg	Enthalpy
					Condensate from Preheater
	0.00	0.27		kg/s	Mass flow
	214.3	238.7		kJ/kg	Enthalpy
					Steam Exit
	0.144	0.190	0.246	Bar	Pressure
	55.0	60.7	66.2	C	Temperature
	4.56	4.48	4.63	kg/s	Mass flow
	2604.2	2613.6	2622.5	kJ/kg	Enthalpy
					Brine Exit
0.144	0.144	0.190	0.246	Bar	Pressure
54.0	55.0	60.7	66.2	C	Temperature
6.00	5.99	5.96	5.93	%	Salt concentration
27.7	27.8	18.9	9.6	kg/s	Mass flow
208.1	212.3	234.8	256.1	kJ/kg	Enthalpy
					Condensate Exit
0.144	0.190	0.190	0.312	Bar	Pressure
53.2	59.0	59.0	70.0	C	Temperature
18.7	14.1	9.6	4.8	kg/s	Mass flow
222.7	246.9	246.8	293.0	kJ/kg	Enthalpy

Table 5. Thermal Balance of the Solar Field Used in MED

		Off-design Heat Balance Results
		Solar Field[6]
	THERMINOL VP-1	Heat transfer fluid type
%	100	HTF concentration
		1. Irradiance

		Irradiance specification: User-defined DNI, site location, and local time
W/m^2	800	Direct normal irradiance
W/m^2	799.7	Aperture normal direct irradiance
Degrees	25.25	Site latitude
Degrees	53.53	Site longitude
hours	3.00	Local time zone (standard time)
	173	Day in standard year
	ژوئن, 22	Date
hours	12.00	Local standard time
Degrees	1.576	Incidence angle
Degrees	258	Solar azimuth angle
Degrees	7.596	Solar zenith angle
Degrees	82.4	Solar altitude angle
Degrees	-7.432	Aperture tracking angle
%	0	Estimated shaded aperture percentage
		2. Heat Balance
kW	13056	Heat transfer to network
		Network inlet:
kg/s	22	Mass flow
bar	31.99	Pressure
C	131.3	Temperature
kJ/kg	636.9	Enthalpy
		Network exit:
kg/s	22	Mass flow
bar	25.77	Pressure
C	398	Temperature
kJ/kg	1230.3	Enthalpy
		Inlet Header:
kg/s	22	Mass flow
bar	31.99	Pressure
C	131.3	Temperature
kJ/kg	636.9	Enthalpy
kW	38.38	Heat loss in header
		Collector Inlet:
kg/s	22	Mass flow
bar	30.44	Pressure
C	130.4	Temperature
kJ/kg	635.1	Enthalpy
m/s	1.375	Inlet tube velocity
		Collector Exit:
kg/s	22	Mass flow
bar	27.32	Pressure
C	399.3	Temperature
kJ/kg	1233.8	Enthalpy
m/s	1.927	Tube velocity at collector exit
		Exit Header:
kg/s	22	Mass flow
bar	25.77	Pressure
C	398	Temperature
kJ/kg	1230.3	Enthalpy
kW	76.76	Heat loss in header
bar	1.551	Inlet header pressure drop

bar	3.114	Collector flowpath pressure drop
bar	1.551	Exit header pressure drop
		3. Summary
	5	Number of operating flow paths
	8	Number of existing flow paths
kg/s	4.4	Mass flow per operating flow path
kg/m^2-s	1339.7	Mass flux
kW	3946	Solar energy impinging focused active aperture in each operating flow path
%	0	Percentage of active aperture in operating flowpaths defocused to control flow or exit state
kW	2808.8	Solar energy absorbed by receiver in each operating flow path
kW	174.6	Energy loss from receiver in each operating flow path
kW	2634.2	Net heat absorbed by fluid in each operating flow path
kW	23.03	Heat loss from inlet and exit headers per operating flow path
kW	13056	Net heat absorbed by field
%	66.76	Collector [excl. headers] efficiency (Fluid heating in receiver / Energy impinging focused active collector)
%	66.17	Field [incl. headers] efficiency (Fluid heating in field / Energy impinging focused active collector)
%	14.36	Area [incl. headers] efficiency (Fluid heating in field / DNI impinging installed area)

Table 6. Hardware Specifications of the Solar Field Used in MED

		Estimated Collector and Field Dimensions
		Solar Field[6]
		1. Reflector Cross Section
		Reflector type: Parabolic trough
%	75	Optical efficiency at 0 degrees incidence
	0.9991	Incident angle optical efficiency factor
	0.95	Reflector cleanliness factor
	0.9999	Reflector end loss factor
%	0	Estimated shaded aperture percentage
mm	70	Receiver outside diameter
mm	2.667	Receiver wall thickness
mm	64.67	Receiver inside diameter
	TP321H	Receiver tube material
mm	136	Receiver glass envelope outside diameter
mm	3	Receiver glass envelope wall thickness
m	5.6	Reflector aperture width
m	1.175	Reflector depth
m	1.668	Reflector focal length
	80	Geometric concentration
Degrees	80	Rim angle
	0.2979	Ratio of reflector focal length to aperture width
		2. Reflector Row (each)
m	14	Row pitch
m	463.8	Row length
m	440.6	Reflector length
m	0.0459	Unused reflector length due to end loss
m^2	2467.5	Reflector aperture area
m^2	2732.3	Reflective area
	2	Number of reflector rows per liquid flow path
		3. Flow Path (each)
mm	70	Receiver tube outside diameter
mm	64.67	Receiver tube inside diameter
mm	2.667	Receiver tube wall thickness
mm	0.0457	Receiver tube internal absolute roughness
m	881.2	Illuminated (heated) length
m	945	Physical length of all straight runs
m	9.441	Equivalent length of all fittings

m	954.4	Total equivalent length
	6	Total number of fittings
	4	Number short 90 deg. Elbows
	2	Number gate valves
		4. Field
	16	Number of reflector rows
	8	Number of liquid flow paths
m^2	39481	Reflector aperture area
m^2	43718	Reflective area
m	14	Row pitch
Degrees	0	Tracking axis rotation away from north
Degrees	0	Tracking axis tilt away from level
m	238	Collector field length perpendicular to tracking axis
m	477.8	Collector field length parallel to tracking axis
m^2	113723	Collector field required land area
hectare	11.37	Collector field required land area

Table 7. Specifications of the MED-Solar Field

		Estimated Collector and Field Data
		Solar Field[6]
		1. Field
	16	Number of reflector rows
m^2	39481	Total active aperture area
m^2	43718	Total reflective area
m	7421	Total receiver length
kg	373522	Total structure weight
l	24373	Volume fluid in tubes
l	36560	Volume fluid in field and related devices
	544	Number foundations
m	238	Collector field length perpendicular to tracking axis
m	477.8	Collector field length parallel to tracking axis
m^2	113723	Collector field required land area
hectare	11.37	Collector field required land area
		2. Reference Material, Equipment, and Installation Costs
		Mechanical
USD	3,690,000	Receiver cost
USD	3,945,000	Reflector cost
USD	6,276,000	Structure, drives, positioning system cost
USD	144,850	Heat transfer fluid cost
USD	2,108,000	Headers, piping, and miscellaneous material and equipment cost
hours	215,200	Mechanical labor
USD	8,607,000	Mechanical labor cost
USD	24,772,000	Reference Mechanical Cost Subtotal
		Civil
m^3	1,410	Foundation concrete volume
USD	594,900	Foundation material and equipment cost
USD	396,200	Excavation/backfill material and equipment cost
hours	19,840	Civil labor
USD	694,300	Civil labor cost
USD	1,685,000	Reference Civil Cost Subtotal
		3. Cost Summary
USD	26,458,000	Total reference installed cost
USD per m^2	605	Total reference installed cost per unit reflective area
USD per m^2	670	Total reference installed cost per unit aperture area
	1	Total installed cost adjustment factor
USD	23,895,000	Total estimated installed cost

Table 8. Steam Turbine MED Parameters

		Off-design Heat Balance Results
		Turbine Inlet
bar	10	Pressure
C	371	Temperature
kg/s	4.346	Massflow
kJ/kg	3203	Enthalpy
		Turbine Outlet
bar	5.2	Pressure
C	296.3	Temperature
kg/s	4.346	Massflow
kJ/kg	3057	Enthalpy
		Performance
%	81.51	Dry step efficiency
%	81.96	Overall apparent isentropic efficiency
kW	629.4	Shaft power
kW	1.261	Mechanical loss
kW	630.7	Expansion power

Table 9. Summary of Solar-MED Costs

	Estimated Cost	Cost Summary
USD	31,499,616	1. Sum of Costs for PEACE Components and Linked GT PRO, GT MASTER & STEAM MASTER Files
USD	0	2. Sum of User-defined Costs
USD	31,499,616	3. Sum of PEACE Components, Linked Files, and User-defined Costs (Contractor's Internal Cost)
USD	1,153,897	Contractor's Soft & Miscellaneous Costs
USD	32,653,513	4. Contractor's Price
USD	2,453,414	Owner's Soft & Miscellaneous Costs
USD	35,106,927	5. Total - Owner's Cost - See Cautionary Note Below
MWe	0.4582	6. Plant Net Electric Output

Table 10. Cost of Solar-MED Components

	Est. Cost	Ref. Cost	Cost Adj. Factor	Unit Cost	Cost Breakdown
USD	31,499,616	33,785,555			Sum of Costs of PEACE Components & Linked Files
USD	4,239,466	4,021,205	1		STAssembly[1]
				4,021,205	Steam Turbine[24]
USD	24,920	39,370			Pipe(PCE)
			1	19,685	Pipe(PCE)[36]
			1	19,685	Pipe(PCE)[37]
USD	2,727,456	2,684,503			MED Desalination
			1	2,684,503	MED Desalination[9]
USD	31,942	32,879			General Pump
			1	32,879	General Pump[1]
USD	114,415	107,354			Shell-Tube Economiser
			1	107,354	Shell-Tube Economiser[7]
USD	216,117	206,499			Shell-Tube Evaporator
			1	206,499	Shell-Tube Evaporator[5]

USD	250,786	236,041			Shell-Tube Superheater
			1	236,041	Shell-Tube Superheater[35]
USD	23,894,520	26,457,700			Solar Field
			1	26,457,700	Solar Field[6]

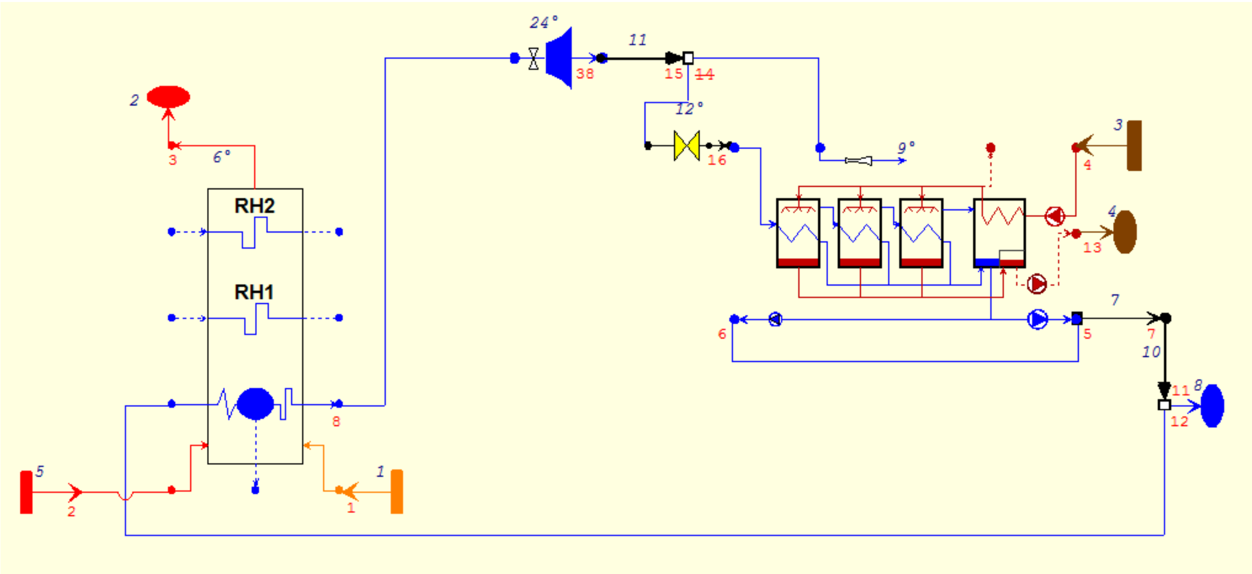

Figure 2. Schematic of the conventional MED system

Table 11. Specifications of the Conventional-MED Boiler Fuel

		Gas Fuel
		Fuel Name: CH4
C	25	Fuel supply temperature
	16.04	Molecular weight
kJ/kg	50047	Total LHV + Sensible heat @ 25C
kJ/kg	55736	Total fuel enthalpy reference to 0C
[kJ/scm]	32824	Volumetric LHV @ 25C (scm: m^3 @ 25 C & 1 atm)
[kJ/scm]	36422	Volumetric HHV @ 25C (scm: m^3 @ 25 C & 1 atm)
		Heating Values
kJ/kg	50047	LHV @ 25C
kJ/kg	55533	HHV @ 25C
		Analysis of Fuel (volume %)
%	0	Hydrogen H2
%	0	Oxygen O2
%	0	Water Vapor H2O
%	0	Nitrogen N2
%	0	Carbon Monoxide CO
%	0	Carbon Dioxide CO2
%	100	Methane CH4
%	0	Ethane C2H6
%	0	Propane C3H8
%	0	n-Butane C4H10
%	0	n-Pentane C5H12
%	0	Hexane C6H14
%	0	Ethylene C2H4
%	0	Propylene C3H6
%	0	Butylene C4H8
%	0	Pentene C5H10
%	0	Benzene C6H6
%	0	Toluene C7H8
%	0	Xylene C8H10
%	0	Acetylene C2H2

%	0	Naphthalene C10H8
%	0	Methanol CH3OH
%	0	Ethanol C2H5OH
%	0	Ammonia NH3
%	0	Hydrogen Sulfide H2S
%	0	Sulfur Dioxide SO2
%	0	Isobutane C4H10
%	0	Carbonyl Sulfide COS
%	0	Hydrogen Cyanide CHN
%	0	Argon Ar
%	100	Total

Table 12. The thermal balance table of the Conventional-MED boiler

		Off-design Heat Balance Results
		Package Boiler(PCE)[1]
	1	Number of Units
	1	Number Units in Operation
		Following quantities in this table are on a per unit basis
		Package Boiler(PCE)[1] - Gaseous fired
%	89.45	Boiler efficiency (LHV_chemical)
%	80.61	Boiler efficiency (HHV_chemical)
%	89.45	Boiler adjusted efficiency (LHV)
%	80.61	Boiler adjusted efficiency (HHV)
%	15	Excess air
		Inlet Air
bar	1.013	Pressure
C	35	Temperature
kg/s	6.032	Mass flow
		Flue Gas
bar	1.013	Pressure
C	237.9	Temperature
kg/s	6.33	Mass flow
%	69.37	Mole percent N2
%	2.428	Mole percent O2
%	8.119	Mole percent CO2
%	19.25	Mole percent H2O
%	0	Mole percent SO2
%	0.8355	Mole percent Ar
		Steam Production
kg/s	4.465	Steam flow
bar	5.72	Pressure
C	371	Temperature
kJ/kg	3209	Enthalpy
		Inlet Water
kg/s	4.476	Mass flow
bar	7.19	Pressure
C	53.35	Temperature
kJ/kg	223.9	Enthalpy
		Blowdown
kg/s	0.0112	Mass flow
bar	5.811	Pressure
C	157.6	Temperature
kJ/kg	665.2	Enthalpy

		Inlet Fuel : Gaseous
kg/s	0.2979	Fuel mass flow
kJ/kg	55533	High heating value
kJ/kg	50047	Low heating value
C	25	Fuel inlet temperature
		Performance
C	1310.2	Furnace exit temperature
%	38.8	Evaporation load in furnace
kW	27.46	FD fan power

Table 13. Specifications of the Conventional-MED Boiler

		Estimated Boiler Data
		Package Boiler(PCE)[1]
USD	1122273	Total Reference Installed Cost
USD	1194316	Total Estimated Installed Cost
	1	Number of Units
		Following quantities in this table are on a per unit basis
		1. Boiler System Summary
	Package Boiler	Boiler Type
kg/s	4.469	Nominal flow
bar	5.5	Nominal pressure
C	371	Nominal steam temperature
m	5.873	Overall length
m	2.908	Overall width
m	3.914	Overall height
kg	31,850	Installed weight
kg	31,010	Boiler weight (dry)
kg	39,350	Boiler weight (wet)
kg	28,490	Package boiler shipping weight
m^2	502	Overall heat transfer surface area
m^2	24.48	- Water wall
m^2	0	- Economiser
m^2	434	- Evaporator (convective)
m^2	43.19	- Superheater (convective & radiant)
		2. Furnace
m	4.179	Furnace length
m	2.603	Furnace height
m	0.2603	Furnace width
m^3	2.832	Furnace volume
		3. Convective Pass
m	5.263	Length (duct length)
m	2.603	Height
m	2.368	Width
		4. Boiler Drum
mm	1,220	Drum outer diameter
mm	610	Low drum outer diameter
m	4.179	Drum length
		5. Boiler Stack
mm	731	Stack diameter
m	5.117	Stack height
kg	838	Stack weight

Table 14. Conventional-MED Water/Steam Table

				Water/Steam Results (per unit)
				Package Boiler(PCE)[1]
Enthalpy	Mass flow	Temperature	Pressure	Stream
kJ/kg	kg/s	C	Bar	
				Water path
223.9	4.476	53.35	7.19	Water inlet
223.9	0.0039	53.35	7.19	Desup water source
223.9	4.472	53.38	5.811	Water after feedwater control valve
				Evaporation and blowdown
665.2	0.0112	157.6	5.811	Blowdown
2754.1	2.73	157.6	5.811	Evaporator exit
2754.1	1.731	157.6	5.811	Radiant Evaporator exit
				Superheating
2754.1	4.461	157.6	5.811	Primary superheater inlet
3212	4.461	372.3	5.72	Primary superheater exit
223.9	0.0039	53.35	7.19	Desup water
3209	4.465	371	5.72	Steam delivery

Table 15. Summary of Costs for Conventional-MED

	Estimated Cost	Cost Summary
USD	8,161,247	1. Sum of Costs for PEACE Components and Linked GT PRO, GT MASTER & STEAM MASTER Files
USD	0	2. Sum of User-defined Costs
USD	8,161,247	3. Sum of PEACE Components, Linked Files, and User-defined Costs (Contractor's Internal Cost)
USD	109,099	Contractor's Soft & Miscellaneous Costs
USD	8,270,346	4. Contractor's Price
USD	245,472	Owner's Soft & Miscellaneous Costs
USD	8,515,818	5. Total - Owner's Cost - See Cautionary Note Below

Table 16. Cost of Conventional-MED Components

	Est. Cost	Ref. Cost	Cost Adj. Factor	Unit Cost	Cost Breakdown
USD	8,161,247	7,827,991			Sum of Costs of PEACE Components & Linked Files
USD	4,239,466	4,021,205	1		STAssembly[1]
				4,021,205	Steam Turbine[24]
USD	1,194,316	1,122,273			Package Boiler(PCE)
			1	1,122,273	Package Boiler(PCE)[1]
USD	2,727,465	2,684,513			MED Desalination
			1	2,684,513	MED Desalination[9]

Table 17. Specifications of the Turbine Set in the MSF Project

		STAssembly[1]
		Estimated Steam Turbine Data
		1. Steam Turbine Description
MVA	12.78	Nameplate Capacity
	0.9	Design Point Generator Power Factor
%	97.17	Design Point Generator Efficiency
	Condensing, Non-Reheat	Steam Turbine Type
bar	10.5	Nameplate Throttle Pressure
C	371	Nameplate Throttle Temperature
kg/s	16.04	Nameplate Throttle Massflow

	Down Draft	Exhaust End Type
	1	Number of LPT Exhaust Annuli
	1	Number of Extraction/Admission Ports
	1	Number of Auto-Extraction/Auto-Admission Ports
		2. Estimated Weights & Dimensions
m	7.243	Steam Turbine Length (including Gear Box)
m	2.993	Steam Turbine Width
kg	42,070	Steam Turbine Weight (including Weight of Gear Box)
m	2.554	Gearbox Length
m	5.843	Generator Length (Including Exciter)
m	2.386	Generator Width
kg	33,050	Generator Weight
m	13.09	Overall ST and Generator Length
m	2.993	Overall ST and Generator Width
kg	75,100	Overall ST and Generator Weight
m	14.9	Foundation Length
m	3.591	Foundation Width
		3. Reference Material, Equipment, and Installation Costs
		Equipment
USD	6,921,000	Steam Turbine Package Cost
		Including:
		- Turbine
		- Generator
		- Gearbox
		- Exhaust System
		- Electrical/Control/Instrumentation Package
		- Lube Oil Package w/ main, auxiliary & emergency pump
		- Transportation to Site
		Mechanical
hours	6,800	Mechanical labor
USD	271,950	Mechanical labor cost
		Transportation & Rigging
USD	78,850	On-site Transportation & Rigging
		Civil (ST and Laydown Pads)
m^3	116	Foundation concrete volume
USD	125,400	Foundation material & equipment cost
m^3	156	Excavation/backfill volume
USD	9,970	Excavation/backfill material and equipment cost
hours	4,690	Civil labor
USD	164,100	Civil labor cost
		5. Cost Summary
USD	7,572,000	Total Reference Installed Cost
	1	Total Installed Cost Adjustment Factor
USD	7,572,000	Total Adjusted Reference Installed Cost
USD	8,085,000	Total Estimated Installed Cost
		STAssembly[1]
		Overall Steam Turbine Thermodynamic Data
		1. Steam Turbine Performance
MWe	10.96	Generator Power
%	97.13	Generator Efficiency
kW	17.26	Lube Oil Pump Auxiliary
kW	23.01	Miscellaneous Auxiliary Power
RPM	3000	Shaft Speed

MWe	11.28	Shaft Power
kW	323.8	Generator Loss
		2. Steam Turbine Main Steam
kg/s	16.04	Mass Flow
bar	10	Pressure
C	371	Temperature
kJ/kg	3203	Enthalpy
		3. Casings
		HPT
MWe	11.28	Casing Shaft Power
%	89.57	Casing Efficiency
		Inlet Steam
kg/s	16.04	Mass Flow
bar	10	Pressure
C	371	Temperature
kJ/kg	3203	Enthalpy
		Exit Steam
kg/s	14.44	Mass Flow
bar	0.0999	Pressure
C	45.82	Temperature
kJ/kg	2426.2	Enthalpy
%	93.38	Quality
ST 11	ST 24	STAssembly[1]
		Steam Turbine Group Data
HPT	HPT	Casing
-	-	Casing Path
		Thermodynamic data
1	1	Number of flow paths
88.95	90.25	Dry step efficiency [%]
89.28	90.66	Group efficiency [%]
3000	3000	Shaft speed [RPM]
19.69	2.921	Mechanical loss [kW]
9824	1457.3	Shaft power [kW]
		Group Inlet
14.32	16.04	Mass flow [kg/s]
7	10	Pressure [bar]
324.7	371	Temperature [C]
3111	3203	Enthalpy [kJ/kg]
1	1	Steam quality
7	10	Pressure after inlet loss [bar]
0	-0.1253	Leakage massflow into group (net) [kg/s]
		Group Exit
14.44	15.91	Mass flow [kg/s]
0.0999	7	Pressure [bar]
45.82	324.7	Temperature [C]
2426.2	3111	Enthalpy [kJ/kg]
0.9338	1	Steam quality
4.585	0	Leaving loss [kJ/kg]
0.1138	0	Leakage massflow into group (net) [kg/s]
		Blading (per flow path)
N/A	0	Number of governing stage rows
N/A	N/A	Governing stage pitch diameter [mm]
7	2	Number of stages

5.565	4.657	Inlet volume flow [m^3/s]
0.016	0.0181	Nozzle area [m^2]
195.7	6.183	Exit volume flow [m^3/s]
1.889	N/A	Annulus area [m^2]
103.6	N/A	Annulus velocity [m/s]
1458	N/A	Last stage pitch diameter [mm]
412.4	N/A	Last stage blade length [mm]
		STAssembly[1]
		Steam Turbine Leakages
		1. Leakages
		Valve Stem leak 1
	SSR	Leakage destination
m^2	1.353	Leakage flow C-factor
kg/s	0.0102	Mass flow
bar	10	Pressure (source)
bar	1.241	Pressure (sink)
C	371	Temperature (source)
C	364.7	Temperature (sink)
kJ/kg	3203	Enthalpy
		HPT HP leak 1
	SSR	Leakage destination
m^2	19.85	Leakage flow C-factor
kg/s	0.1151	Mass flow
bar	7.692	Pressure (source)
bar	1.241	Pressure (sink)
C	369.3	Temperature (source)
C	364.7	Temperature (sink)
kJ/kg	3203	Enthalpy
		2. Sealing Steam Regulator (SSR)
bar	1.241	Pressure
C	148.9	Temperature
kg/s	0.1453	Total mass flow
kJ/kg	2771.9	Enthalpy
		Leakage In
		Valve Stem leak 1
kg/s	0.0102	Mass flow
kJ/kg	3203	Enthalpy
		HPT HP leak 1
kg/s	0.1151	Mass flow
kJ/kg	3203	Enthalpy
		Make-up Steam (from HPT inlet)
kg/s	0	Mass flow
		Desuperheating water
kg/s	0.0199	Mass flow
kJ/kg	62.8	Enthalpy
		LPT sealing Steam to LPT exhaust
kg/s	0.0504	Mass flow
		LPT sealing Steam Packing Exhaust
kg/s	0.0315	Mass flow
		Packing Exhaust destination
		Discharged
		Excess Sealing Steam
	LPT exhaust	Destination
kg/s	0.0634	Mass flow

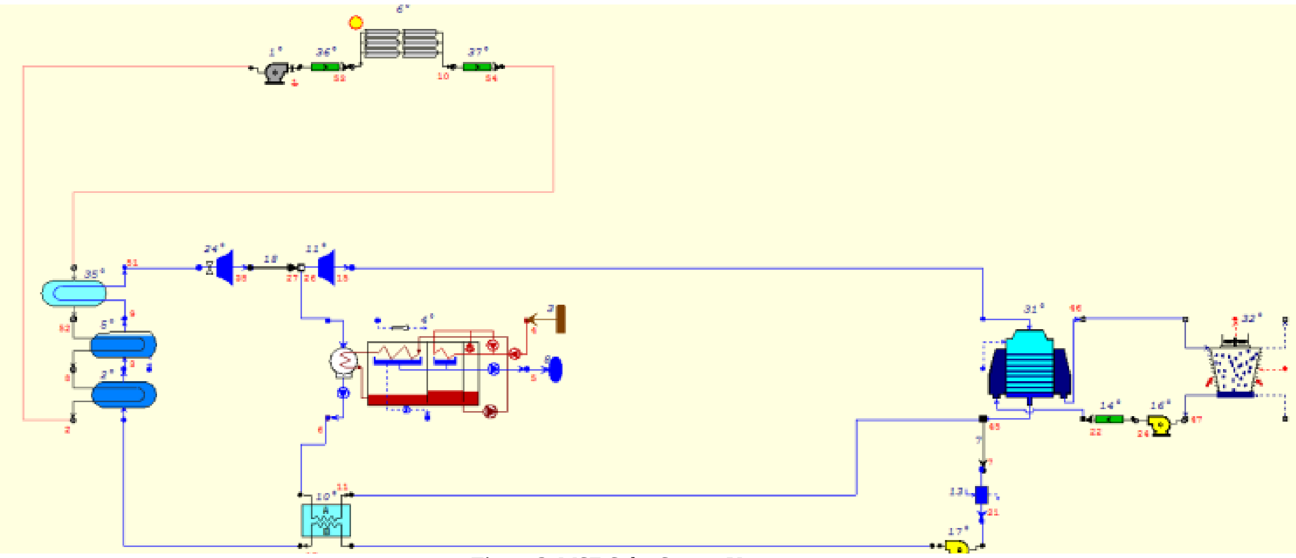

Figure 3. MSF-Solar System View

Table 18. Thermal Balance of Solar MSF

		Off-design Heat Balance Results
		MSF Desalination[4]
	1	Number of units
	8.725	Gain output ratio (desalinated water / steam flow)
	7.711	Performance ratio (kg/2325.9kJ)
		Desalinated Water
bar	1.014	Pressure
C	37.76	Temperature
kJ/kg	158.2	Enthalpy
kg/s	13.88	Mass flow (per unit)
MIGD	0.2646	Volume flow (MIGD per unit)
m^3/day	1203	Volume flow (m^3/day per unit)
		Heating Steam
bar	6.5	Pressure
C	324.2	Temperature
kJ/kg	3111	Enthalpy
kg/s	1.591	Mass flow (per unit)
		Desuperheating Water (from Brine Heater Condensate)
kg/s	0.2889	Mass flow (per unit)
kJ/kg	479	Enthalpy
		Steam at Brine Heater Inlet
bar	1.645	Pressure
C	119.2	Temperature
kJ/kg	2706.3	Enthalpy
kg/s	1.88	Mass flow (per unit)
bar	1.645	Brine Heater Condensing Pressure
C	114.2	Brine Heater Condensing Temperature
		Brine Heater Condensate
bar	0.468	Pressure
C	114.2	Temperature
kJ/kg	479	Enthalpy
kg/s	1.88	Mass flow (per unit, before desuperheating)
kg/s	1.591	Mass flow (per unit, after desuperheating)

		Cold Brine at HGS Inlet
bar	5.464	Pressure
C	40.27	Temperature
%	4.971	Salt concentration
kJ/kg	157.8	Enthalpy
kg/s	123.9	Mass flow (per unit)
		Brine Heater Inlet (Cold Brine at HGS Exit)
bar	2.249	Pressure
C	101.5	Temperature
%	4.971	Salt concentration
kJ/kg	399.7	Enthalpy
kg/s	123.9	Mass flow (per unit)
		Brine Heater Exit
bar	2.155	Pressure
C	110	Temperature
%	4.971	Salt concentration
kJ/kg	433.5	Enthalpy
kg/s	123.9	Mass flow (per unit)
		Hot Brine at HGS Inlet
bar	2.247	Pressure
C	110	Temperature
%	4.971	Salt concentration
kJ/kg	433.5	Enthalpy
kg/s	123.9	Mass flow (per unit)
		Hot Brine at HGS Exit
bar	0.1076	Pressure
C	48.99	Temperature
%	5.518	Salt concentration
kJ/kg	190.1	Enthalpy
kg/s	111.6	Mass flow (per unit)
		Hot Brine at Last Stage Exit
bar	0.0665	Pressure
C	39.99	Temperature
%	5.6	Salt concentration
kJ/kg	154.7	Enthalpy
kg/s	110	Mass flow (per unit)
		Seawater Supply
bar	1.014	Pressure
C	25	Temperature
%	4	Salt concentration
kJ/kg	99	Enthalpy
kg/s	74.64	Mass flow (per unit)
		Seawater Discharge
bar	1.014	Pressure
C	39.99	Temperature
%	4	Salt concentration
kJ/kg	158.6	Enthalpy
kg/s	26.04	Mass flow (per unit)
		Makeup Seawater (from HRS Tube Side Outlet)
C	39.99	Temperature
kJ/kg	158.6	Enthalpy

kg/s	48.59	Mass flow (per unit)
		Seawater Recirculation
kg/s	37.24	Mass flow (per unit)
		Brine Blowdown
bar	1.014	Pressure
C	40.05	Temperature
%	5.6	Salt concentration
kJ/kg	155.1	Enthalpy
kg/s	34.71	Mass flow (per unit)
		Chemical Consumption (100% equivalent)
kg/hr	0.4373	Anti-scale
kg/hr	0.035	Anti-foam
kg/hr	6.123	Sulfuric acid
kg/hr	0.4998	Caustic soda
kg/hr	0.1999	Chlorine
USD	47989	Total O&M cost per year
		Heat Transfer Data
		Brine Heater
W/m^2-C	2285.3	Overall heat transfer coefficient
m^2-C/W	0.1585 x 10^-3	Fouling resistance
		Heat recovery section condensers
W/m^2-C	2239.4	Overall heat transfer coefficient (average)
m^2-C/W	0.1585 x 10^-3	Fouling resistance
		Heat rejection section condensers
W/m^2-C	1607.7	Overall heat transfer coefficient (average)
m^2-C/W	0.1937 x 10^-3	Fouling resistance
kW	180.3	Power Consumption (plant total)
kW	180.3	Power Consumption (per unit)
kW	159.1	Pump total
kW	22.94	Seawater Supply Pump
kW	104.1	Brine Recirculation Pump
kW	15.2	Brine Blowdown Pump
kW	4.699	Desalinated Water Pump
kW	0	Brine Heater Condensate Pump
kW	12.15	Seawater Recirculation Pump
kW	21.17	Miscellaneous auxiliaries
kW	12471	Energy In (per unit)
kW	4950	Heating steam
kW	7389	Seawater supply
kW	131.8	Pump work
kW	12471	Energy Out (per unit)
kW	762.3	Brine Heater condensate
kW	4129	Seawater discharge
kW	2197.1	Desalinated water
kW	5383	Blowdown
kW	0	High purity water
%	-0.0014	Heat Balance Error

Table 19. MSF Specifications

		Estimated Multi-Stage Flash (MSF) Desalination System Data
		MSF Desalination[4]
	Off Design	Computation mode
		1. General
	1	Number of units
	21	Number of stages per unit
	18	Number of stages in heat recovery section (HGS)
	3	Number of stages in heat rejection section (HRS)
kg/s	13.85	Nominal desalinated water flow per unit
MIGD	0.264	Nominal desalinated water flow per unit (MIGD)
m^3/day	1200	Nominal desalinated water flow per unit (m^3/day)
		2. Overall dimensions and total weight (per unit, excluding seawater supply circuit)
m	17.21	Length
m	9.244	Width
m	1.409	Height
tonne	67.46	Dry weight
		3. Brine heater (per unit)
	CuNi 70-30	Tube material
m^2	239.7	Heat transfer area
mm	15.88	Tube outside diameter
mm	1	Tube wall thickness
m	7.11	Tube length
	676	Number of tubes
		4. Evaporator (per unit)
m	13.83	Length
m	6.099	Width
m	0.9396	Height
tonne	51.89	Dry weight
		HGS Stage Condensers
	CuNi 90-10	- Tube material
m^2	139	- Heat transfer area per stage
m^2	2502.3	- HGS total heat transfer area
mm	15.88	- Tube outside diameter
mm	1	- Tube wall thickness
m	6.099	- Tube length
	457	- Number of tubes per stage
		HRS Stage Condensers
	Titanium	- Tube material
m^2	161.5	- Heat transfer area per stage
m^2	484.6	- HRS total heat transfer area
mm	15.88	- Tube outside diameter
mm	0.7	- Tube wall thickness
m	6.099	- Tube length
	531	- Number of tubes per stage
		5. Cost Summary
USD	3,243,134	Total reference installed cost
	1	Total installed cost adjustment factor
USD	3,295,024	Total estimated installed cost

Table 20. Thermal Balance of the Solar Field in the MSF-Solar System

		Off-design Heat Balance Results
		Solar Field[6]
	THERMINOL VP-1	Heat transfer fluid type
%	100	HTF concentration

		1. Irradiance
		Irradiance specification: User-defined DNI, site location, and local time
W/m^2	800	Direct normal irradiance
W/m^2	799.7	Aperture normal direct irradiance
Degrees	25.25	Site latitude
Degrees	53.53	Site longitude
hours	3.00	Local time zone (standard time)
	173	Day in standard year
	22 ,ژوئن	Date
hours	12.00	Local standard time
Degrees	1.576	Incidence angle
Degrees	258	Solar azimuth angle
Degrees	7.596	Solar zenith angle
Degrees	82.4	Solar altitude angle
Degrees	-7.432	Aperture tracking angle
%	0	Estimated shaded aperture percentage
		2. Heat Balance
kW	48180	Heat transfer to network
		Network inlet:
kg/s	82.5	Mass flow
bar	32.09	Pressure
C	132.2	Temperature
kJ/kg	638.4	Enthalpy
		Network exit:
kg/s	82.5	Mass flow
bar	25.54	Pressure
C	395	Temperature
kJ/kg	1222.4	Enthalpy
		Inlet Header:
kg/s	82.5	Mass flow
bar	32.09	Pressure
C	132.2	Temperature
kJ/kg	638.4	Enthalpy
kW	143.9	Heat loss in header
		Collector Inlet:
kg/s	82.5	Mass flow
bar	30.54	Pressure
C	131.2	Temperature
kJ/kg	636.7	Enthalpy
m/s	1.434	Inlet tube velocity
		Collector Exit:
kg/s	82.5	Mass flow
bar	27.1	Pressure
C	396.3	Temperature
kJ/kg	1225.9	Enthalpy
m/s	1.997	Tube velocity at collector exit
		Exit Header:
kg/s	82.5	Mass flow
bar	25.54	Pressure
C	395	Temperature
kJ/kg	1222.4	Enthalpy
kW	287.8	Heat loss in header

bar	1.551	Inlet header pressure drop
bar	3.443	Collector flowpath pressure drop
bar	1.551	Exit header pressure drop
		3. Summary
	18	Number of operating flow paths
	27	Number of existing flow paths
kg/s	4.583	Mass flow per operating flow path
kg/m^2-s	1395.5	Mass flux
kW	4042	Solar energy impinging focused active aperture in each operating flow path
%	0	Percentage of active aperture in operating flowpaths defocused to control flow or exit state
kW	2877	Solar energy absorbed by receiver in each operating flow path
kW	176.3	Energy loss from receiver in each operating flow path
kW	2700.6	Net heat absorbed by fluid in each operating flow path
kW	23.99	Heat loss from inlet and exit headers per operating flow path
kW	48180	Net heat absorbed by field
%	66.82	Collector [excl. headers] efficiency (Fluid heating in receiver / Energy impinging focused active collector)
%	66.23	Field [incl. headers] efficiency (Fluid heating in field / Energy impinging focused active collector)
%	16	Area [incl. headers] efficiency (Fluid heating in field / DNI impinging installed area)

Table 21. MSF-Solar Field Hardware

		Estimated Collector and Field Dimensions
		Solar Field[6]
		1. Reflector Cross Section
		Reflector type: Parabolic trough
%	75	Optical efficiency at 0 degrees incidence
	0.9991	Incident angle optical efficiency factor
	0.95	Reflector cleanliness factor
	0.9999	Reflector end loss factor
%	0	Estimated shaded aperture percentage
mm	70	Receiver outside diameter
mm	2.667	Receiver wall thickness
mm	64.67	Receiver inside diameter
	TP321H	Receiver tube material
mm	136	Receiver glass envelope outside diameter
mm	3	Receiver glass envelope wall thickness
m	5.6	Reflector aperture width
m	1.175	Reflector depth
m	1.668	Reflector focal length
	80	Geometric concentration
Degrees	80	Rim angle
	0.2979	Ratio of reflector focal length to aperture width
		2. Reflector Row (each)
m	14	Row pitch
m	475.1	Row length
m	451.3	Reflector length
m	0.0459	Unused reflector length due to end loss
m^2	2527.4	Reflector aperture area
m^2	2798.6	Reflective area
	2	Number of reflector rows per liquid flow path
		3. Flow Path (each)
mm	70	Receiver tube outside diameter
mm	64.67	Receiver tube inside diameter
mm	2.667	Receiver tube wall thickness
mm	0.0457	Receiver tube internal absolute roughness
m	902.5	Illuminated (heated) length

m	967.5	Physical length of all straight runs
m	9.441	Equivalent length of all fittings
m	976.9	Total equivalent length
	6	Total number of fittings
	4	Number short 90 deg. Elbows
	2	Number gate valves
		4. Field
	54	Number of reflector rows
	27	Number of liquid flow paths
m^2	136482	Reflector aperture area
m^2	151127	Reflective area
m	14	Row pitch
Degrees	0	Tracking axis rotation away from north
Degrees	0	Tracking axis tilt away from level
m	770	Collector field length perpendicular to tracking axis
m	489.1	Collector field length parallel to tracking axis
m^2	376593	Collector field required land area
hectare	37.66	Collector field required land area

Table 22. Specifications of MSF-Solar Field

		Estimated Collector and Field Data
		Solar Field[6]
		1. Field
	54	Number of reflector rows
m^2	136482	Total active aperture area
m^2	151127	Total reflective area
m	25654	Total receiver length
kg	1291230	Total structure weight
l	84255	Volume fluid in tubes
l	126382	Volume fluid in field and related devices
	1890	Number foundations
m	770	Collector field length perpendicular to tracking axis
m	489.1	Collector field length parallel to tracking axis
m^2	376593	Collector field required land area
hectare	37.66	Collector field required land area
		2. Reference Material, Equipment, and Installation Costs
		Mechanical
USD	8,495,000	Receiver cost
USD	9,081,000	Reflector cost
USD	14,447,000	Structure, drives, positioning system cost
USD	500,800	Heat transfer fluid cost
USD	4,879,000	Headers, piping, and miscellaneous material and equipment cost
hours	495,350	Mechanical labor
USD	19,813,000	Mechanical labor cost
USD	57,216,000	Reference Mechanical Cost Subtotal
		Civil
m^3	4,890	Foundation concrete volume
USD	2,067,000	Foundation material and equipment cost
USD	1,377,000	Excavation/backfill material and equipment cost
hours	68,900	Civil labor
USD	2,412,000	Civil labor cost
USD	5,856,000	Reference Civil Cost Subtotal
		3. Cost Summary
USD	63,071,000	Total reference installed cost
USD per m^2	417	Total reference installed cost per unit reflective area
USD per m^2	462	Total reference installed cost per unit aperture area

	1	Total installed cost adjustment factor
USD	56,932,000	Total estimated installed cost

Table 23. Summary of MSF-Solar Costs

	Estimated Cost	Cost Summary
USD	71,463,320	1. Sum of Costs for PEACE Components and Linked GT PRO, GT MASTER & STEAM MASTER Files
USD	0	2. Sum of User-defined Costs
USD	71,463,320	3. Sum of PEACE Components, Linked Files, and User-defined Costs (Contractor's Internal Cost)
USD	3,838,923	Contractor's Soft & Miscellaneous Costs
USD	75,302,240	4. Contractor's Price
USD	6,431,699	Owner's Soft & Miscellaneous Costs
USD	81,733,940	5. Total - Owner's Cost - See Cautionary Note Below
MWe	10.24	6. Plant Net Electric Output

Table 24. Cost of MSF-Solar Components

	Est. Cost	Ref. Cost	Cost Adj. Factor	Unit Cost	Cost Breakdown
USD	71,463,320	77,003,190			Sum of Costs of PEACE Components & Linked Files
USD	8,084,535	7,571,567	1		STAssembly[1]
					Steam Turbine[24]
					Steam Turbine[11]
USD	121,639	118,463			Pump(PCE)
			1	85,895	Pump(PCE)[16]
			1	32,568	Pump(PCE)[17]
USD	764,578	757,643			Water-cooled Condenser(PCE)
			1	757,643	Water-cooled Condenser(PCE)[31]
USD	758,687	739,591			Wet Cooling Tower(PCE)
			1	739,591	Wet Cooling Tower(PCE)[32]
USD	175,147	241,472			Pipe(PCE)
			1	166,940	Pipe(PCE)[14]
			1	32,253	Pipe(PCE)[36]
			1	42,278	Pipe(PCE)[37]
USD	3,295,024	3,243,134			MSF Desalination
			1	3,243,134	MSF Desalination[4]
USD	217,522	204,912			General Pump
			1	204,912	General Pump[1]
USD	190,481	179,483			Shell-Tube Economiser
			1	179,483	Shell-Tube Economiser[7]
USD	388,174	371,581			Shell-Tube Evaporator
			1	371,581	Shell-Tube Evaporator[5]
USD	535,456	504,060			Shell-Tube Superheater
			1	504,060	Shell-Tube Superheater[35]
USD	56,932,080	63,071,290			Solar Field
			1	63,071,290	Solar Field[6]

					Makeup/Blowdown
				not included	Makeup/Blowdown[13]

Table 25. Thermal Balance of the Conventional-MSF Boiler

		Off-design Heat Balance Results
		Package Boiler(PCE)[5]
	1	Number of Units
	1	Number Units in Operation
		Following quantities in this table are on a per unit basis
		Package Boiler(PCE)[5] - Gaseous fired
%	94.6	Boiler efficiency (LHV_chemical)
%	85.25	Boiler efficiency (HHV_chemical)
%	94.39	Boiler adjusted efficiency (LHV)
%	85.08	Boiler adjusted efficiency (HHV)
%	15	Excess air
		Inlet Air
bar	1.013	Pressure
C	40.18	Temperature
kg/s	20.2	Mass flow
		Flue Gas
bar	1.013	Pressure
C	133	Temperature
kg/s	21.2	Mass flow
%	69.34	Mole percent N2
%	2.328	Mole percent O2
%	8.165	Mole percent CO2
%	19.34	Mole percent H2O
%	0	Mole percent SO2
%	0.835	Mole percent Ar
		Steam Production
kg/s	15.93	Steam flow
bar	9	Pressure
C	371	Temperature
kJ/kg	3204	Enthalpy
		Inlet Water
kg/s	15.97	Mass flow
bar	10.81	Pressure
C	53.01	Temperature
kJ/kg	222.7	Enthalpy
		Blowdown
kg/s	0.0398	Mass flow
bar	9.198	Pressure
C	176.3	Temperature
kJ/kg	747	Enthalpy
		Inlet Fuel : Gaseous
kg/s	1.004	Fuel mass flow
kJ/kg	55533	High heating value
kJ/kg	50047	Low heating value
C	25	Fuel inlet temperature
		Performance
C	1022.3	Furnace exit temperature

%	60	Evaporation load in furnace
kW	136.5	FD fan power
		Flue Gas Recirculation
	Boiler outlet	FGR source
	FD Fan inlet	FGR sink
kg/s	1.031	FGR flow

Table 26. Specifications of the Conventional-MSF Boiler

		Estimated Boiler Data
		Package Boiler(PCE)[5]
USD	2539869	Total Reference Installed Cost
USD	2672928	Total Estimated Installed Cost
	1	Number of Units
		Following quantities in this table are on a per unit basis
		1. Boiler System Summary
	Package Boiler	Boiler Type
kg/s	15.93	Nominal flow
bar	9	Nominal pressure
C	371	Nominal steam temperature
m	11.09	Overall length
m	4.29	Overall width
m	5.454	Overall height
kg	93,650	Installed weight
kg	91,400	Boiler weight (dry)
kg	112,900	Boiler weight (wet)
kg	73,950	Package boiler shipping weight
m^2	1,890	Overall heat transfer surface area
m^2	147	- Water wall
m^2	837	- Economiser
m^2	744	- Evaporator (convective)
m^2	162	- Superheater (convective & radiant)
		2. Furnace
m	9.874	Furnace length
m	4.143	Furnace height
m	2.391	Furnace width
m^3	97.81	Furnace volume
		3. Convective Pass
m	10.49	Length (duct length)
m	4.143	Height
m	1.631	Width
		4. Boiler Drum
mm	1,220	Drum outer diameter
mm	610	Low drum outer diameter
m	9.874	Drum length
		5. Boiler Stack
mm	1,190	Stack diameter
m	8.364	Stack height
kg	2,270	Stack weight

Table 27. Specifications of Conventional-MSF Steam/Water

				Water/Steam Results (per unit)
				Package Boiler(PCE)[5]
Enthalpy	Mass flow	Temperature	Pressure	Stream
kJ/kg	kg/s	C	bar	
				Water path
222.7	15.97	53.01	10.81	Water inlet
222.7	15.97	53.03	9.43	Economiser inlet
417.8	15.97	99.54	9.198	Economiser exit
				Evaporation and blowdown
747	0.0398	176.3	9.198	Blowdown
2772.9	6.372	176.3	9.198	Evaporator exit
2772.9	9.558	176.3	9.198	Radiant Evaporator exit
				Superheating
2772.9	15.93	176.3	9.198	Primary superheater inlet
3204	15.93	371	9	Primary superheater exit
3204	15.93	371	9	Steam delivery

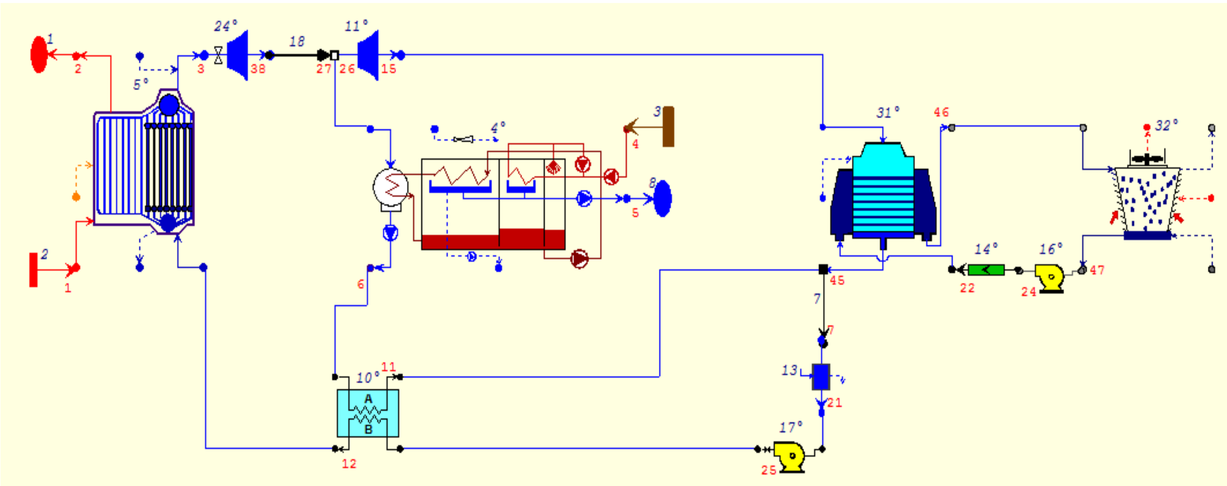

Figure 4. Schematic of the MSF - Conventional Boiler System

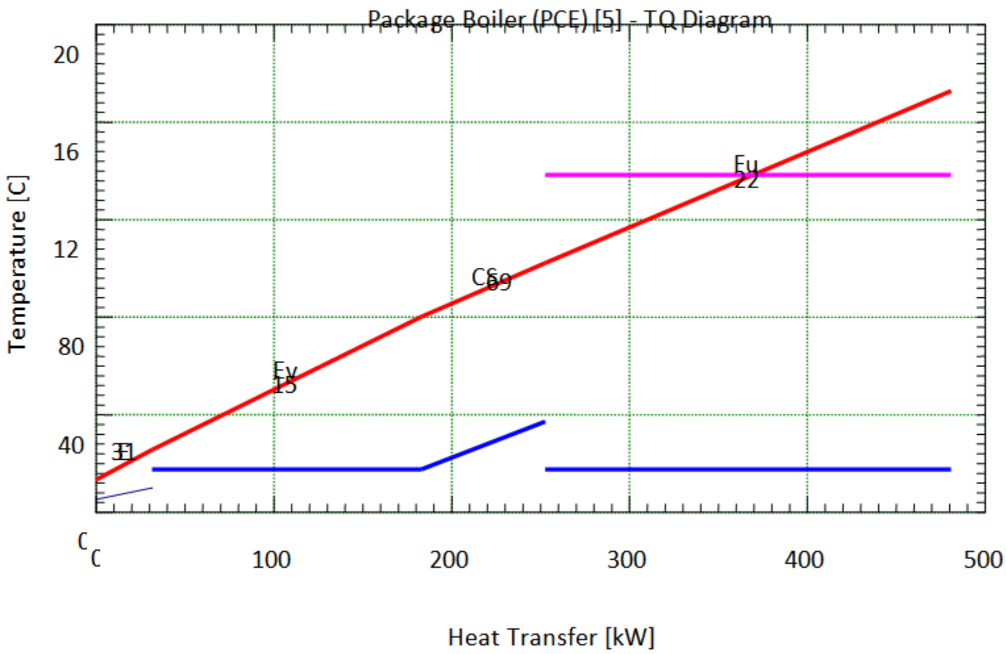

Figure 5. T_Q Diagram

Table 28. Summary of Costs for Conventional-MSF

	Estimated Cost	Cost Summary
USD	15,593,040	1. Sum of Costs for PEACE Components and Linked GT PRO, GT MASTER & STEAM MASTER Files
USD	0	2. Sum of User-defined Costs
USD	15,593,040	3. Sum of PEACE Components, Linked Files, and User-defined Costs (Contractor's Internal Cost)
USD	1,461,390	Contractor's Soft & Miscellaneous Costs
USD	17,054,430	4. Contractor's Price
USD	1,403,373	Owner's Soft & Miscellaneous Costs
USD	18,457,800	5. Total - Owner's Cost - See Cautionary Note Below
MWe	10.06	6. Plant Net Electric Output

Table 29. Cost Breakdown of Conventional-MSF Components

	Est. Cost	Ref. Cost	Cost Adj. Factor	Unit Cost	Cost Breakdown
USD	15,593,040	14,919,560			Sum of Costs of PEACE Components & Linked Files
USD	7,967,883	7,464,833	1		STAssembly[1]
					Steam Turbine[24]
					Steam Turbine[11]
USD	121,717	118,573			Pump(PCE)
			1	85,676	Pump(PCE)[16]
			1	32,897	Pump(PCE)[17]
USD	763,314	756,382			Water-cooled Condenser(PCE)
			1	756,382	Water-cooled Condenser(PCE)[31]
USD	756,823	737,736			Wet Cooling Tower(PCE)
			1	737,736	Wet Cooling Tower(PCE)[32]
USD	124,986	166,940			Pipe(PCE)
			1	166,940	Pipe(PCE)[14]
USD	3,185,386	3,135,223			MSF Desalination
			1	3,135,223	MSF Desalination[4]
USD	2,672,928	2,539,869			Package Boiler(PCE)
			1	2,539,869	Package Boiler(PCE)[5]
					Makeup/Blowdown
				not included	Makeup/Blowdown[13]

3.2. Sensitivity Analysis

Based on the calculations performed and the results obtained in the previous section, this section focuses on the sensitivity analysis of the parameters influencing the system's efficiency. In this section, the sensitivity of output parameters to several input parameters is examined to determine the optimal operating condition of the system. The criterion for assessing the sensitivity of the system's input parameters is the overall efficiency of the system. The sensitivity results are presented for the following parameters in Tables 29 to 35 and their corresponding Figure 6 to Figure 12.

Ambient temperature plays a critical role in system performance, significantly influencing key parameters. As ambient temperature increases, net power output and net electric efficiency improve slightly, reflecting the system's ability to adapt positively to higher temperatures. This enhancement indicates stable performance under varying thermal conditions. Simultaneously, both net heat rate and gross heat rate decrease, signifying improved thermal efficiency as the system consumes less energy per unit of power generated. However, this comes with a slight increase in net fuel input, as higher energy demands are required to sustain the increased power output. In addition, the ambient wet bulb temperature rises directly with ambient temperature, highlighting its dependence on environmental conditions and its potential impact on the performance of cooling systems. Overall, higher ambient temperatures lead to improved efficiency and power generation but come at the cost of slightly increased fuel consumption. These results underscore the importance of considering ambient temperature in the optimal design and operation of systems to balance efficiency and energy use effectively.

The sensitivity analysis results of the power generation system indicate that variations in the sodium chloride (NaCl) weight percentage, ranging from 3.5% to 4.5%, have a notable yet limited impact on system performance, while other environmental conditions, including ambient pressure (1.013 bar), ambient temperature (35°C), relative humidity (60%), and wet bulb temperature (28.18°C), remain constant. The gross power output shows a marginal increase from 598.8 kW to 599.3 kW with the rise in NaCl concentration, reflecting the low sensitivity of gross power to this parameter. Similarly, the net power output increases from 457.8 kW to 458.6 kW, indicating a positive but minor influence of NaCl concentration on the system's net output. Net electric efficiency exhibits a slight improvement from 16.506% to 16.513%, underscoring the beneficial impact of NaCl percentage on system efficiency, albeit modest. Furthermore, the net heat rate decreases progressively from 102672 kJ/kWh to 102482 kJ/kWh, highlighting an enhancement in energy utilization efficiency as the NaCl concentration increases. Conversely, the net fuel input remains constant at 13056 kW across all cases, indicating no direct dependency of fuel consumption on NaCl concentration.

This study examines the effect of brine source temperature on system performance, with the temperature varying from 15°C (Case 1) to 40°C (Case 6) while keeping ambient conditions, including pressure, temperature, and relative humidity, constant. The results indicate that increasing the brine source temperature leads to a rise in gross power output from 583.3 kW to 622.8 kW and net power output from 442.6 kW to 481.6 kW, reflecting enhanced system performance at higher temperatures. Similarly, net electric efficiency improved from 16.388% to 16.693%, demonstrating better energy conversion efficiency. Furthermore, the net heat rate decreased from 106,264 kJ/kWh to 97,487 kJ/kWh, indicating reduced energy consumption per unit of power generation. Notably, the net fuel input remained nearly constant, with only minor variations from 13,064 kW to 13,042 kW. These findings underscore the positive impact of higher brine source temperatures on overall system efficiency, as evidenced by increased power output and improved net electric efficiency, accompanied by a reduction in net heat rate, all without significant changes in fuel consumption. Therefore, utilizing higher-temperature sources can be considered an effective strategy to enhance system efficiency.

Based on the obtained data, the solar field mass flow is the only variable input parameter that changed within the range of 12 to 20 kg/s. However, this variation had no significant impact on the main output parameters. The gross and net power outputs, which remained constant at 599 kW and 458.2 kW respectively across all cases, indicate that changes in the solar field mass flow did not affect the system's power generation. Furthermore, the net electric efficiency of the system consistently remained at 16.51%, demonstrating no effect of mass flow variations on system efficiency. The net heat rate exhibited very minor variations within a narrow range of 102574 to 102576 kJ/kWh, reflecting negligible sensitivity of this parameter to changes in the solar field mass flow. Similarly, the net fuel input remained constant at 13056 kW in all scenarios, indicating that increases in solar field mass flow did not influence fuel consumption. Overall, the results indicate that the system, under the analyzed conditions, shows low sensitivity to variations in solar field mass flow. Its performance, including power generation and efficiency, remained stable across different mass flow rates. Only minor changes in the net heat rate were observed, which can be considered negligible.

The results of this study indicate that increasing the solar field outlet temperature has a positive impact on system performance. As the outlet temperature rises from 380°C to 420°C, the gross power output increases from 594 kW to 605.1 kW, while the net power output improves from 451.3 kW to 466.3 kW, reflecting enhanced energy production and system efficiency. The net electric efficiency, based on the lower heating value (LHV), also increases from 16.442% to 16.594%, signifying improved energy conversion efficiency. Furthermore, the net heat rate decreases from 104,593 kJ/kWh to 100,174 kJ/kWh, demonstrating enhanced thermodynamic performance. In addition, the net fuel input decreases from 13,113 kW to 12,975 kW, indicating reduced fuel consumption and higher system efficiency. These findings underscore that increasing the solar field outlet temperature significantly enhances the system's overall performance in all critical aspects, highlighting the importance of optimizing outlet temperature to achieve maximum operational efficiency.

Based on the sensitivity analysis results, it is evident that the highest net power output occurs in Case 4 (456.7 kW), indicating optimal system performance under these conditions. Conversely, the lowest net power output is observed in Case 3 (395.4 kW), which may be attributed to operational limitations or specific conditions in this scenario. The net electric efficiency is highest in Cases 4 and 5, with values of 16.502% and 16.451%, respectively, reflecting the efficient utilization of fuel energy in these cases. On the other hand, the lowest efficiency is recorded in Cases 1 and 8, with values of 16.05% and 16.01%. In terms of fuel consumption, the highest input is observed in Cases 4 and 5 (13039 and 12928 kW, respectively), consistent with their higher net power output. The lowest fuel consumption occurs in Cases 1 and 8 (7216 and 7198 kW), indicating lower energy demand in these conditions. Furthermore, the lowest net heat rate is recorded in Cases 1 and 8 (65340 and 65183 kJ/kWh), signifying more efficient energy conversion in these cases. Conversely, the highest net heat rate is observed in Case 3 (111983 kJ/kWh), which correlates with the system's lower efficiency in this scenario. Environmental parameters such as pressure, temperature, and relative humidity remain constant across all cases, and the observed variations in results are primarily attributed to internal system parameters and temporal conditions (day of the year). Overall, Case 4 demonstrates the best performance in terms of power output and efficiency, albeit with higher fuel consumption. In contrast, Cases 1 and 8 exhibit more optimized fuel consumption and heat rates but generate lower net power. The selection of the optimal scenario depends on operational priorities, particularly whether the goal is to maximize efficiency or minimize fuel consumption. These findings can provide valuable insights for future decision-making to optimize system performance.

The performance analysis of the system under various operational conditions indicates that despite constant environmental parameters such as pressure, temperature, and relative humidity, significant variations in power output and system efficiency are observed across different scenarios. Among all scenarios, Case 3 demonstrates the highest net power output of 460 kW, while Case 5 records the lowest at 387.4 kW. Additionally, the net electric efficiency reaches its peak in Case 3 at 16.518%, reflecting the system's optimal performance, whereas Case 5 exhibits the lowest efficiency at 16.122%, indicating a noticeable decline in system performance. The net heat rate also achieves its most efficient value in Case 3 at 102333 kJ/kWh, highlighting the optimal energy utilization in this case, while Case 5 shows an anomalously low value of 40402 kJ/kWh, signaling significant operational issues requiring further investigation. Regarding fuel consumption, Case 3 reports the highest value at 13075 kW, whereas Case 5 has the lowest at 4348 kW. Gross power output follows a similar trend, with Case 3 reaching the highest value of 600.9 kW, and Case 5 the lowest at 518.1 kW. Overall, this sensitivity analysis underscores the substantial impact of slight changes in operational parameters on the system's overall performance and emphasizes the critical need for precise management and optimization of operating conditions.

Table 30. Sensitivity analysis to ambient temperature ranging from 15 to 45°C

Ambient temperature	C	15	22.5	30	37.5	45
Ambient RH	%	60	60	60	60	60
Ambient wet bulb temperature	C	10.82	17.31	23.82	30.37	36.98
Gross heat rate(LHV)	kJ/kWh	78621	78565	78504	78441	78376
Net power	kW	455.9	456.7	457.6	458.5	459.4
Net electric efficiency(LHV)	%	16.499	16.502	16.507	16.511	16.515
Net heat rate(LHV)	kJ/kWh	102897	102784	102662	102538	102412
Net fuel input(LHV)	kW	13032	13040	13049	13059	13069

Table 31. Sensitivity Analysis of Seawater Salinity Percentage

PLANT SUMMARY	Unit	Case 1	Case 2	Case 3	Case 4	Case 5
Computation Result Messages		Messages	Messages	Messages	Messages	Messages
Ambient pressure	bar	1.013	1.013	1.013	1.013	1.013
Ambient temperature	C	35	35	35	35	35
Ambient RH	%	60	60	60	60	60
NaCl weight percent	%	3.5	3.75	4	4.25	4.5
Ambient wet bulb temperature	C	28.18	28.18	28.18	28.18	28.18
Gross power	kW	598.8	598.9	599	599.2	599.3
Net power	kW	457.8	458	458.2	458.4	458.6
Net electric efficiency(LHV)	%	16.506	16.508	16.51	16.511	16.513
Net heat rate(LHV)	kJ/kWh	102672	102623	102574	102530	102482
Net fuel input(LHV)	kW	13056	13056	13056	13056	13056

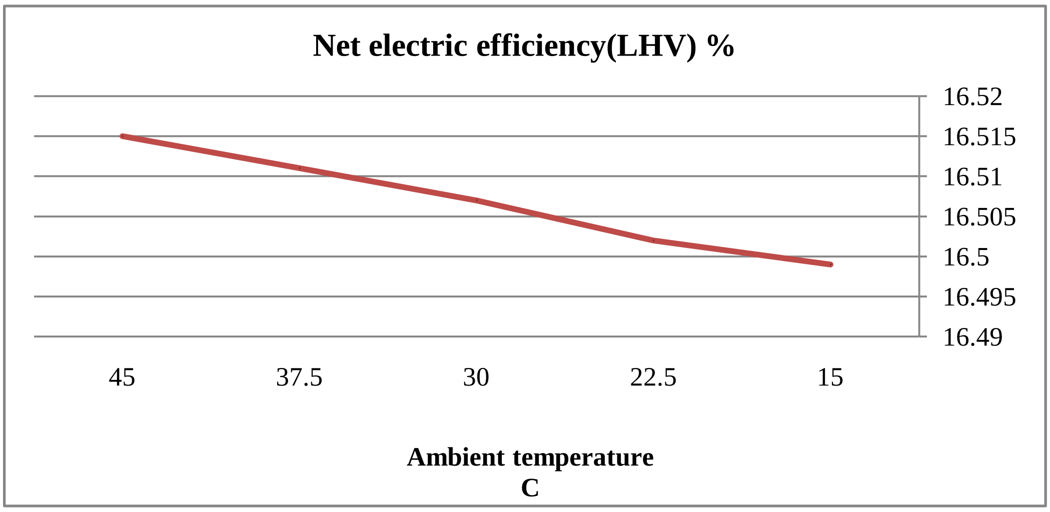

Figure 6. Sensitivity Analysis to Ambient Temperature

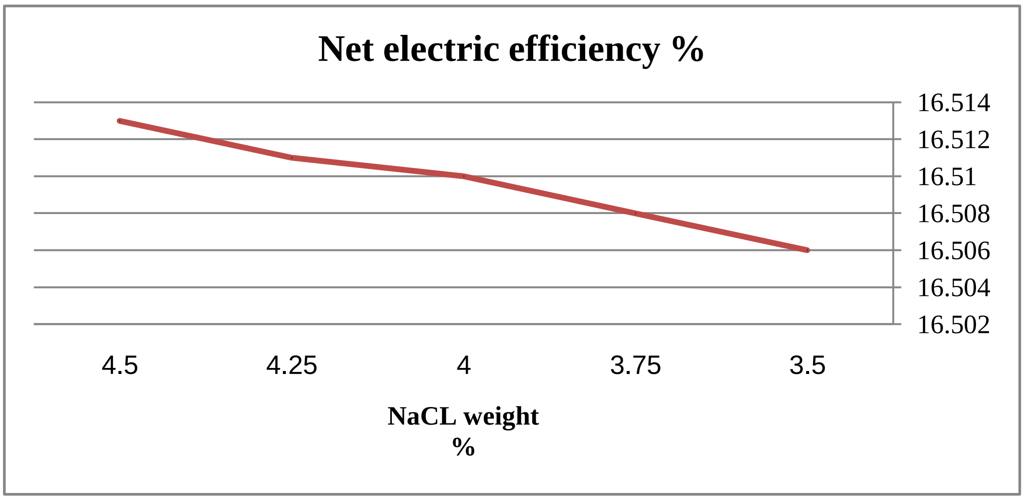

Figure 7. Sensitivity Analysis of Salt Percentage

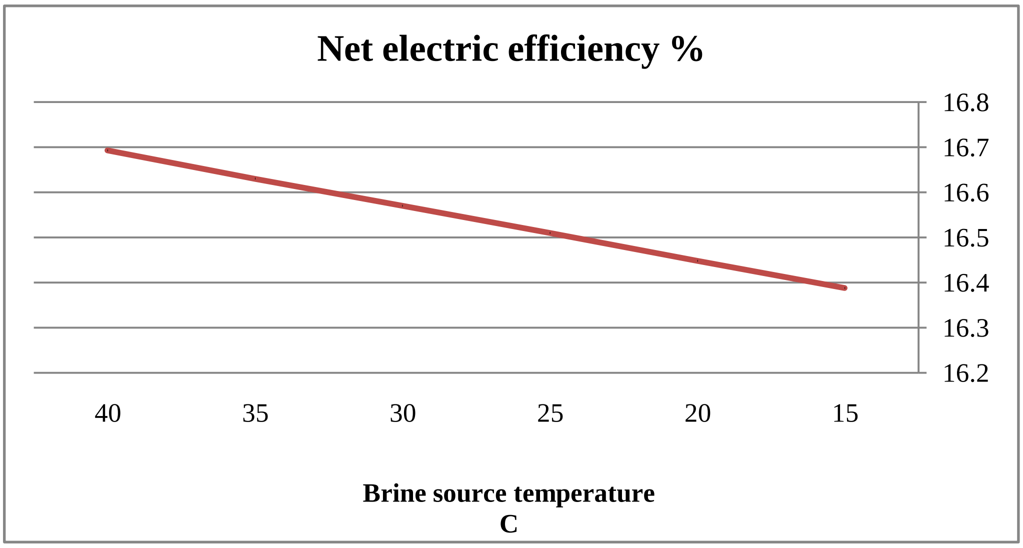

Figure 8. Sensitivity Analysis of Sea Water Temperature

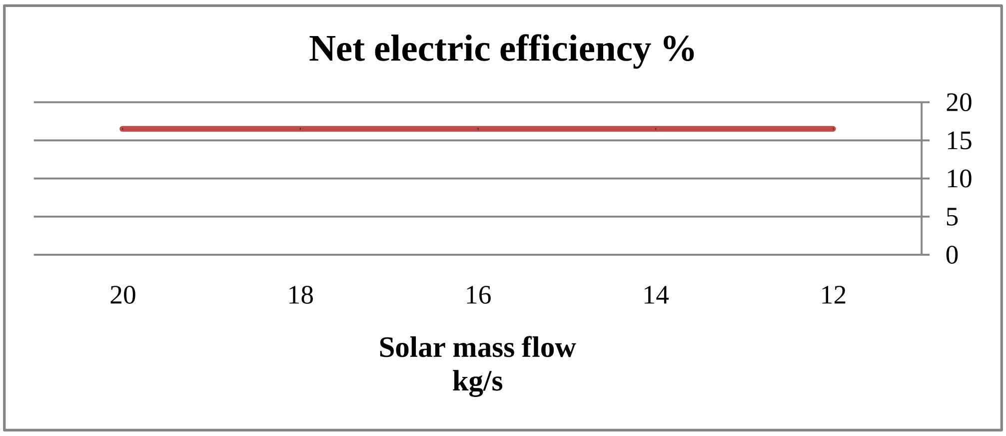

Figure 9. Sensitivity Analysis of the Output Flow Rate of the Solar Field

Table 32. Sensitivity Analysis of Sea Water Temperature

PLANT SUMMARY	Unit	Case 1	Case 2	Case 3	Case 4	Case 5	Case 6
Computation Result Messages		Messages	Messages	Messages	Messages	Messages	Messages
Ambient pressure	bar	1.013	1.013	1.013	1.013	1.013	1.013
Ambient temperature	C	35	35	35	35	35	35
Ambient RH	%	60	60	60	60	60	60
Ambient wet bulb temperature	C	28.18	28.18	28.18	28.18	28.18	28.18
Brine source temperature	C	15	20	25	30	35	40

Gross power	kW	583.3	591.1	599	606.8	614.7	622.8
Net power	kW	442.6	450.3	458.2	465.9	473.6	481.6
Net electric efficiency(LHV)	%	16.388	16.448	16.51	16.57	16.63	16.693
Net heat rate(LHV)	kJ/kWh	106264	104411	102574	100854	99166	97487
Net fuel input(LHV)	kW	13064	13060	13056	13051	13047	13042

Table 33. Sensitivity Analysis of the Output Flow Rate of the Solar Field

PLANT SUMMARY	Unit	Case 1	Case 2	Case 3	Case 4	Case 5
Computation Result Messages		Messages	Messages	Messages	Messages	Messages
Ambient pressure	bar	1.013	1.013	1.013	1.013	1.013
Ambient temperature	C	35	35	35	35	35
Ambient RH	%	60	60	60	60	60
Ambient wet bulb temperature	C	28.18	28.18	28.18	28.18	28.18
Solar field mass flow	kg/s	12	14	16	18	20
Gross power	kW	599	599	599	599	599
Net power	kW	458.2	458.2	458.2	458.2	458.2
Net electric efficiency(LHV)	%	16.51	16.51	16.51	16.51	16.51
Net heat rate(LHV)	kJ/kWh	102574	102574	102576	102575	102576
Net fuel input(LHV)	kW	13056	13056	13056	13056	13056

Table 34. Sensitivity Analysis of the Output Temperature of the Solar Field

Ambient pressure	bar	1.013	1.013	1.013	1.013	1.013
Ambient temperature	C	35	35	35	35	35
Ambient RH	%	60	60	60	60	60
Ambient wet bulb temperature	C	28.18	28.18	28.18	28.18	28.18
Solar field output temperature	C	380	390	400	410	420
Gross power	kW	594	596.6	599.4	602.2	605.1
Net power	kW	451.3	455	458.8	462.4	466.3
Net electric efficiency(LHV)	%	16.442	16.478	16.516	16.554	16.594
Net heat rate(LHV)	kJ/kWh	104593	103505	102399	101303	100174
Net fuel input(LHV)	kW	13113	13082	13049	13013	12975

Table 35. presents the sensitivity analysis for the day under consideration

PLANT SUMMARY	Unit	Case 1	Case 2	Case 3	Case 4	Case 5	Case 6	Case 7	Case 8
Result Messages		Messages	Messages	Messages	Messages	Messages	Messages	Messages	Messages
Ambient pressure	bar	1.013	1.013	1.013	1.013	1.013	1.013	1.013	1.013
Ambient temperature	C	35	35	35	35	35	35	35	35
Ambient RH	%	60	60	60	60	60	60	60	60
Ambient wet bulb temperature	C	28.18	28.18	28.18	28.18	28.18	28.18	28.18	28.18
Day of the year		1	46	92	137	183	229	274	365
Gross power	kW	528.2	532.3	534.5	597.5	586.7	533.9	530.9	528.1
Net power	kW	397.6	397.8	395.4	456.7	446.2	396.4	398.2	397.6
Net electric efficiency(LHV)	%	16.05	16.1	16.215	16.502	16.451	16.444	16.13	16.01
Net heat rate(LHV)	kJ/kWh	65340	87171	111983	102792	104314	104541	77323	65183
Net fuel input(LHV)	kW	7216	9633	12301	13039	12928	11511	8553	7198

Table 36. Sensitivity Analysis of the Hour Under Review

PLANT SUMMARY	Unit	Case 1	Case 2	Case 3	Case 4	Case 5
Computation Result Messages		Messages	Messages	Messages	Messages	Failed
Ambient pressure	bar	1.013	1.013	1.013	1.013	1.013
Ambient temperature	C	35	35	35	35	35
Ambient RH	%	60	60	60	60	60
Ambient wet bulb temperature	C	28.18	28.18	28.18	28.18	28.18
Hour		7	10	13	16	19
Gross power	kW	557.5	600.7	600.9	554.6	518.1
Net power	kW	417.7	459.8	460	414.9	387.4
Net electric efficiency(LHV)	%	16.309	16.517	16.518	16.295	16.122
Net heat rate(LHV)	kJ/kWh	108780	102358	102333	109254	40402
Net fuel input(LHV)	kW	12621	13074	13075	12591	4348

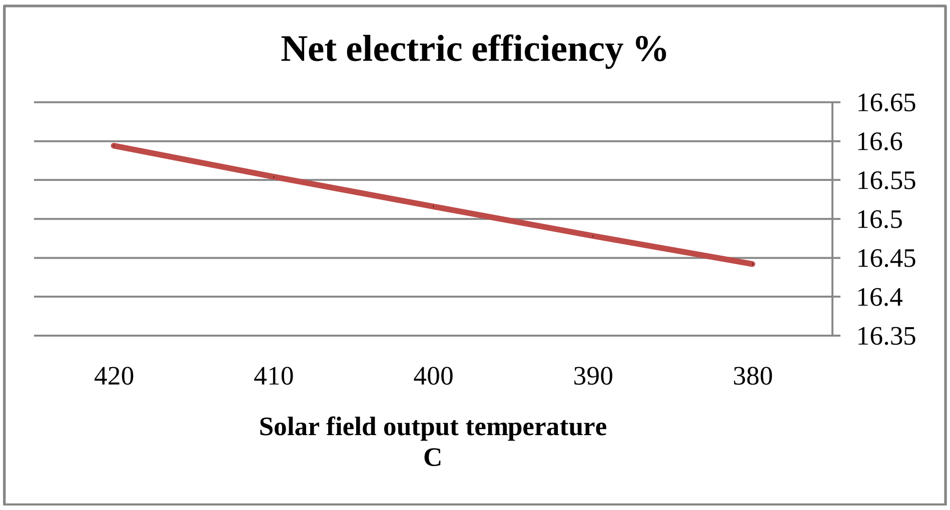

Figure 10. Sensitivity Analysis of the Output Temperature of the Solar Field

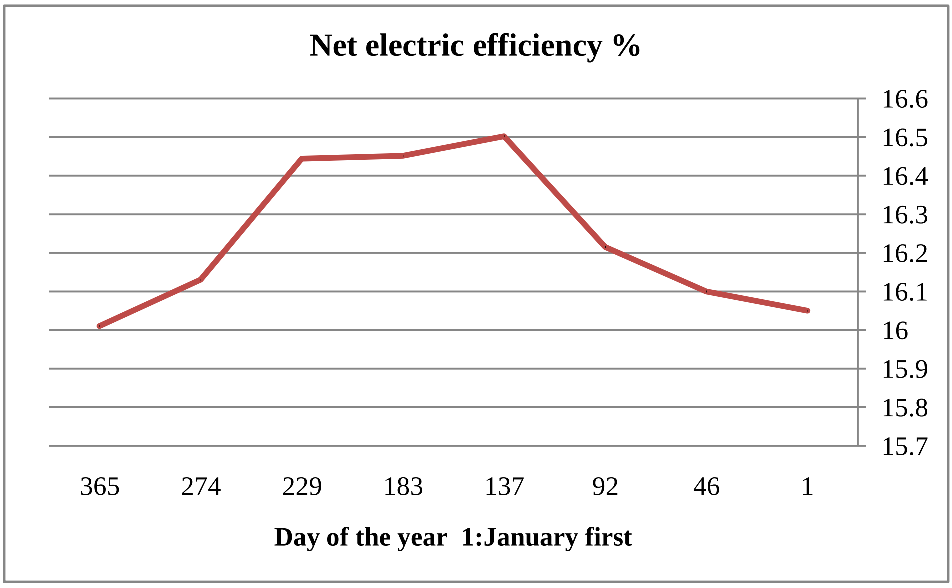

Figure 11. Sensitivity analysis of the day under consideration

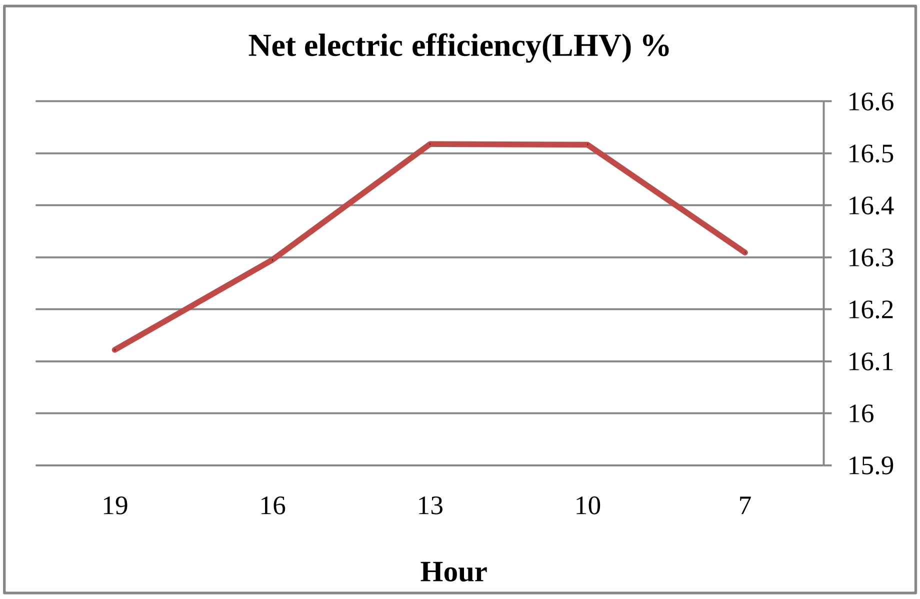

Figure 12. Sensitivity Analysis of the Hour Under Review

4. Conclusion

This study evaluated the performance of MED and MSF desalination systems utilizing a combination of solar energy and conventional boilers. The findings revealed that the selection of the system type and energy source directly influences freshwater production costs, energy efficiency, and environmental sustainability. Among the systems analyzed, the MED-Solar Field system emerged as an economical and sustainable option, with a production cost of $3.22 per cubic meter in the first year, alongside a significant reduction in pollutant emissions. Similarly, the MED-Conventional Boiler system, with a production cost of $1.55 per cubic meter in the first year, was identified as a more economical alternative but remains dependent on fossil fuels. In contrast, MSF systems, due to their high energy demands and substantial initial investments, were deemed more suitable for larger-scale projects with specific applications. Although the MSF-Solar Field system demonstrated favorable technical performance, its high production cost ($7.93 per cubic meter in the first year) and greater initial capital requirements diminished its economic feasibility. The MSF-Conventional Boiler system, with a production cost of $4.66 per cubic meter in the first year and a high boiler efficiency (85%), exhibited reasonable cost performance. However, the environmental impacts of fossil fuel dependency remain a critical challenge for this system. This study also revealed that climatic conditions and environmental variables, including the day of the year, time of day, seawater inlet temperature, and ambient temperature, play a significant role in enhancing the efficiency of solar systems. Specifically, the day of the year and time of day have a substantial impact on cycle performance due to variations in the intensity and angle of solar radiation. Moreover, an increase in ambient temperature and the collector outlet temperature directly improves system efficiency. In contrast, the solar cycle flow rate and salt concentration exhibit no significant effect on system efficiency and can be considered less critical factors in the design process. Overall, the results of this research can serve as a guideline for the optimal selection and design of desalination systems under varying climatic conditions, with an emphasis on utilizing renewable energy sources and reducing operational costs. These findings also provide a valuable foundation for the development of innovative technologies in the management of water and energy resources.

Declaration of Interest Statement

The authors declare that they have no known competing financial interests or personal relationships that could have appeared to influence the work reported in this paper

References

[1] Alhaj, M., Hassan, A., Darwish, M., & Al-Ghamdi, S. G. (2017). A techno-economic review of solar-driven multi-effect distillation. Desal. Wat. Treat., 90(1), 86–98.

[2] Elsheikh, A.H., El-Said, E.M.S., Abd Elaziz, M., Fujii, M., El-Tahan, H.R., 2023. Water distillation tower: Experimental investigation, economic assessment, and performance prediction using optimized machine-learning model. J. Clean. Prod. 388, 135896.

[3] Zanjirabadi, H. R., Saberi, F., Rahimzadeh, B., Masoudi, F., & Rahgosha, M. (2024). Petrology Investigation of Apatite Minerals in the Esfordi Mine, Yazd, Iran. *International Journal of Geological and Environmental Engineering*, *18*(4), 118-124.

[4] Mani, A., 1982. Experimental studies on single sloped solar still. Indian Institute of Technology Madras.

[5] Mani, A., 2018. Technical report on solar multi-effect desalination system. Ministry of Earth Sciences, New Delhi.

[6] Alsaiari, A.O., Moustafa, E.B., Alhumade, H., Abulkhair, H., Elsheikh, A., 2023. A coupled artificial neural network with artificial rabbits optimizer for predicting water productivity of different designs of solar stills. Adv. Eng. Softw. 175, 103315.

[7] Bouchekima, B. (2002). A solar desalination plant for domestic water needs in arid areas of south Algeria. Desalination, 153(1), 65–69.

[8] Moustafa, E.B., Hammad, A.H., Elsheikh, A.H., 2022. A new optimized artificial neural network model to predict thermal efficiency and water yield of tubular solar still. Case Stud. Therm. Eng. 30, 101750.

[9] Saberi, F., Asoude, P., & Abdollahzadeh Bina, F. (2024, July). Sedimentary Environment, Diagenesis of Sarvak Formation in the Zagros Basin, Iran. In *2nd International Congress on Science, Engineering & New Technologies Hamburg, Germany* (pp. 11-13).

[10] Saberi, F., & Hosseini-Barzi, M. (2024). Effect of thermal maturation and organic matter content on oil shale fracturing. *International Journal of Coal Science & Technology*, *11*(1), 16.

[11] Larki, E., Jaffarbabaei, B., Soleimani, B., Elyasi, A., Saberi, F., Makarian, E., ... & Radwan, A. E. (2024). A new insight to access carbonate reservoir quality using quality factor and velocity deviation log. *Acta Geophysica*, *72*(5), 3159-3178.

[12] Barati, M. B., Kadkhodaie, A., Soleimani, B., Saberi, F., & Asoude, P. (2023). Determination of reservoir parameters of the upper part of Dalan formation using NMR log and core in south pars oil field. *Journal of Petroleum Research*, *33*(1402-1), 73-83.

[13] Abbasi, V., Ahmadi, M., Mohtarami, E., Karimi, J., & Saberi, F. (2024). Experimental and numerical failure mechanism evaluation of anisotropic rocks using extended finite element method. *Theoretical and Applied Fracture Mechanics*, *131*, 104411.

[14] Hashemi, R., Saberi, F., Asoude, P., & Soleimani, B. (2024). Enhancing Reservoir Zonation through Triple Porosity System: A Case Study. *SPE Journal*, 1-20.

[15] Elyasi, A., Makarian, E., & Saberi, F. (2023). Fracture gradient prediction: Applicable to safe drilling and underground storage operations. In Proceedings of the 7th International Conferences on Applied Research in Science and Engineering (1-14). London: Institution of Engineering and Technology of London.

[16] Al Mutawa, A. M., Ruwaili, Waleed Mohamed Al Al Murbati, N. A., Al Oraifi, A. S., Al Oraifi, A., Al Arafati, A., Nasrullah, A., ... Al Moosa, S. Z. (2014). Desalination in the GCC the History, the Present & the Future.

[17] Makarian, E., Elyasi, A., & Saberi, F. Geo-Sequestration of Acid Gas (H2S-CO2).

[18] Tay, J.H., Low, S.C., Jeyaseelan, S., 1996. Vacuum desalination for water purification using waste heat. Desalination 106, 131–135.

[19] Low, S.C., Tay, P.J.H., 1991. Vacuum desalination using waste heat from a steam turbine. Desalination 81, 321–331.

[20] Senthil Kumar, R., Kumaraswamy, S., Mani, A., 2007. Experimental investigations on a two-phase jet pump used in desalination systems. Desalination 204, 437–447.

[21] Ahmed, D.S., Mohammed, B.K., Mohammed, M.K.A., 2021. Long-term stable and hysteresis-free planar perovskite solar cells using green antisolvent strategy. J. Mater. Sci. 56, 15205–15214.

[22] Naji, A.M., Kareem, S.H., Faris, A.H., Mohammed, M.K.A., 2021. Polyaniline polymer-modified ZnO electron transport material for high-performance planar perovskite solar cells. Ceram. Int. 47, 33390–33397.

[23] Hassan Kareem, S., Harjan Elewi, M., Muhson Naji, A., Ahmed, D.S., Mohammed, K.A., M., 2022. Efficient and stable pure α-phase FAPbI3 perovskite solar cells with a dual engineering strategy: Additive and dimensional engineering approaches. Chem. Eng. J. 443, 136469.

[24] Fakhri, F., Mansourian, D., Baghishani, H., Elyasi, A., Makarian, E., & Saberi, F. (2025). Innovative numerical techniques for calculating rock strength characteristics: Leveraging integrated machine learning and geostatistical methods. *Geomechanics and Engineering*, *40*(3), 205.

[25] Chaibi, M. T. (2000). An overview of solar desalination for domestic and agriculture water needs in remote arid areas. Desalination, 127(2), 119–133.

[26] Sagie, D., Feinerman, E., & Aharoni, E. (2001). Potential of solar desalination in Israel and in its close vicinity. Desalination, 139(1–3), 21–33.

[27] Saberi, F., Vashaghian, S., Gyimah, E., & Olusegun, T. (2023). Investigating the fractures of asmari formation as a geothermal reservoir with image log. *GRC Transactions*, *47*(1), 3118-3125.

[28] Palenzuela, P., Alarcón-Padilla, D. C., & Zaragoza, G. (2015). Large-scale solar desalination by combination with CSP: Techno-economic analysis of different options for the Mediterranean Sea and the Arabian Gulf. Desalination, 366, 130–138.

[29] Ali, M. T., Fath, H. E. S., & Armstrong, P. R. (2011). A comprehensive techno-economical review of indirect solar desalination. Renewable and Sustainable Energy Reviews, 15(8), 4187–4199.

[30] Bandelier, P., Pelascini, F., d'Hurlaborde, J. J., Maisse, A., Boillot, B., & Laugier, J. (2016). MED seawater desalination using a low-grade solar heat source. Desalination and Water Treatment, 57(48-49), 23074-23084.

[31] Buros, O. K. (1999). The ABCs of desalting (2nd edition). Topsfield, Massachusetts, USA: International Desalination Association.

[32] Casimiro, S., Cardoso, J., Ioakimidis, C., Mendes, J. F., Mineo, C., Cipollina, A., ... Mendes, J. F. (2015). MED parallel system powered by concentrating solar power (CSP). Model and case study: Trapani, Sicily. Desalination and Water Treatment, 55:12, 3253–3266.

[33] Kalogirou, S. A. (2005). Seawater desalination using renewable energy sources. Progress in Energy and Combustion Science, 31(3), 242–281.

[34] Sharaf, M. A., Nafey, A. S., & García-Rodríguez, L. (2011). Exergy and thermo-economic analyses of a combined solar organic cycle with multi effect distillation (MED) desalination process. Desalination, 272(1), 135–147

[35] El-Nashar, A. M. (2001). The economic feasibility of small solar MED seawater desalination plants for remote arid areas. Desalination, 134(1), 173–186.

[36] Palenzuela, P., Hassan, A. S., Zaragoza, G., & Alarcón-Padilla, D.-C. (2014). Steady state model for multi-effect distillation case study: Plataforma Solar de Almería MED pilot plant. Desalination, 337, 31–42.

[37] Saberi, F., Vashaghian, S., Asoudeh, P., & Radwan, A. E. (2024). Computational fluid dynamics study to access the effect of non-Newtonian fluid flow variables on drilling mud in annular oil well. *Improved Oil and Gas Recovery*, *8*.

[38] Saberi, F., Hosseini-Barzi, M., Asoude, P., Bina, F. A., & Radwan, A. E. (2025). Sedimentary facies and depositional-diagenetic model of storm-influenced carbonate ramp system, Paleocene–Oligocene of Pabdeh Formation, Zagros, Iran. *Carbonates and Evaporites*, *40*(2), 41.

[39] Vashaghian, S., Gyimah, E., Olusegun, T., & Saberi, F. (2023). Petro-physical Characterization of Lodgepole Formation as a Geothermal Reservoir. *GRC Trans*, *47*, 3138-3152.

[40] Bataineh, K. M. (2016). Multi-effect desalination plant combined with thermal compressor driven by steam generated by solar energy. Desalination, 385, 39-52.

[41] https://www.naftnews.ir.

[42] Behrooz Heidari Dehkordi, Fatemeh Saberi, Abtin Ataei, Hossein Salehfar, and Farhad Abdollahzadeh Bina, "Optimum Model of a Solar Desalination System Based on Multi-effect Distillation (Solar-MED), Iran."

[43] Kohlin, L., Pritchard, H., Gladen, A. C., Dehkordi, B., & Bajwa, D. (2024). Molten salt biomass torrefaction–A sensitivity analysis of process conditions. *Industrial Crops and Products*, *219*, 118997.

[44] Kohlin, L., Pritchard, H., Gladen, A. C., Dehkordi, B., & Bajwa, D. (2024). Molten salt biomass torrefaction–A sensitivity analysis of process conditions. *Industrial Crops and Products*, *219*, 118997.

[45] Bina, F. A., Satkin, M., & Shabnavard, A. (2020). Recent Attainments and Regulations in the Field of Geothermal Energy in Iran. In *Proceedings World Geothermal Congress*(p. 1).

[46] Porkhial, S., Abdollahzadeh Bina, F., Radmehr, B., & Johari Sefid, P. (2015). Interpretation of the injection and heat up tests at Sabalan geothermal field, Iran. In *Proceedings world geothermal congress* (pp. 19-25).

© The Author(s) 2025. This article is an open access article distributed under the terms and conditions of the Creative Commons Attribution (CC BY) license (http://creativecommons.org/licenses/by/4.0/).